Journal of Fluids and Structures 124 (2024) 104035

Contents lists available at ScienceDirect

Journal of Fluids and Structures

journal homepage: www.elsevier.com/locate/jfs

Observed wake branches from the 2-DOF forced motion of a circular cylinder in a free stream

Erdem Aktosun [a,c], Ersegun D. Gedikli [b], Jason M. Dahl [a,*]

[a] Department of Ocean Engineering, University of Rhode Island, 215 S Ferry Road, Narragansett, 02881, RI, USA
[b] Department of Ocean and Resources Engineering, University of Hawaii at Manoa, 2500 Campus Rd, Honolulu, 96822, HI, USA
[c] Department of Shipbuilding and Ocean Engineering, İzmir Kâtip Çelebi University, Havaalanı Sosesi Cd., Izmir, 35620, Turkey

ARTICLE INFO

Keywords:
2-DOF forced VIV
Flow-structure interactions
Vortex dynamics

ABSTRACT

The combined in-line (IL) and cross flow (CF) vibration of flexibly mounted cylinders in a free stream due to vortex-induced vibration (VIV) demonstrates significantly more complex dynamics than purely CF vibrations. In this study, the forces on a circular cylinder undergoing combined IL and CF motion in a free stream are investigated through an expansive series of forced motion experiments with force measurement and quantitative flow visualization. The motion of the cylinder is parameterized using sinusoidal motions with variation of the non-dimensional IL amplitude, non-dimensional CF amplitude, CF reduced velocity, and phase between IL and CF motion, while the Reynolds number is held constant at 7620. The resulting database of experimental measurements consists of 9555 variations of the governing motion parameters. The decomposed force coefficients are reported and mapped over the range of parameters. We observe a number of interesting wake-dependent parameter space features, such as regions of multiple branch responses, where the wake may exhibit multiple mode behaviors for the same cylinder motion parameters. Multiple branch regions are observed throughout the experimental data space.

1. Introduction

The canonical problem of fluid flow across an elastically mounted circular cylinder has been a widely studied problem in fluid mechanics due to the ubiquitous nature of the simple geometry in engineering applications and the resulting complexity of the fluid–structure interaction (FSI). In many engineering design and operation applications, it is advantageous to be able to predict FSI such as self-limiting VIV, since these vibrations can strongly affect fatigue life or operational downtime in a variety of systems (e.g. motion of offshore structures, vibration of towed cables, loading on mooring systems, vibration of ship appendages, operation of heat exchangers, operation of drilling risers, operation of sub-sea pipelines, etc.). While the vibration of physical continuous systems is complex, where many modes of the system may interact with the surrounding fluid wake, simplifications are often made to understand the relevant physics of the canonical problem. In the case of VIV, one often considers a cylinder that moves perpendicular relative to the direction of the current, shedding a vortex street wake that in turn affects the forces exerted on the cylinder. A variety of reviews have documented the phenomenon of VIV, particularly focusing on the problem of a circular cylinder constrained to move perpendicular to the direction of the current, either through forced motion or freely responding to the hydrodynamic forces (Sarpkaya, 1979; Bearman, 1984; Sarpkaya, 2004; Williamson and Govardhan, 2004), while more recent studies have illustrated

* Corresponding author.
E-mail address: jmdahl@uri.edu (J.M. Dahl).

https://doi.org/10.1016/j.jfluidstructs.2023.104035
Received 6 January 2023; Received in revised form 2 September 2023; Accepted 20 November 2023

effects of combined IL and CF motion on the system response and forces (Bearman, 2011; Triantafyllou et al., 2016; Wang et al., 2020; Fan and Triantafyllou, 2022).

The forces exerted on a circular cylinder undergoing oscillatory motion in a free stream are necessary for understanding the basic physics of the problem and also necessary as an input for any algorithm developed to predict these motions. In general, for an elastically mounted structure with a natural frequency, as vortices are shed into the wake of the structure, they exert a force on the structure, causing it to move. The movement of the structure, in turn, results in additional generation of vorticity that is shed to the wake. The interplay of this phenomenon leads to the self-excitation and vibration of the elastically mounted structure. Early studies on investigating forces on cylinders undergoing oscillatory motions focused on direct measurement of forces and the development of physics-based models to predict these forces under different oscillatory conditions.Bishop and Hassan (1964a,b) was an early study focused on measurement of lift and drag forces, which have been used as a basis for modeling fluid forces on cylinders, particularly in dynamic oscillator models (Gabbai and Benaroya, 2005), which utilize phenomenological equations to approximate the behavior of VIV. In contrast, semi-empirical models, such as those used in the comparison study of Chaplin et al. (2005), utilize direct measurement of fluid forces obtained by parameterizing the kinematics of cylinder motions and conducting a series of forced motion experiments to obtain a parameterized database of force measurements as a function of cylinder kinematics.

An early example of this type of forced motion experiment was Gopalkrishnan (1993), who conducted a series of forced motion experiments where a cylinder was towed at constant forward speed while undergoing a forced oscillation perpendicular to the towing direction. The motion was parameterized as a sinusoidal motion and the amplitude and frequency of motion were varied, while measurement of the forces exerted on the body was made. While a sinusoidal forced motion is an approximation of the true motions that a cylinder experiences when undergoing VIV, semi-empirical methods that utilize this approximation have been shown to be relatively good predictors of forces and motions, at least in the case of a cylinder oscillating perpendicular to the flow direction (Chaplin et al., 2005). The measured forces from this study were normalized into force coefficients and projected into forces in phase with the velocity of the body (excitation), denoted at C_{lv} for lift in phase with velocity, and forces in phase with acceleration of the body (effective added mass), denoted as C_{my} for added mass in the lift (y) direction. These linear projections of the measured force on body motions allow for characterization of regions over which excitation of a flexibly mounted structure may occur and how the effective natural frequency of the system may change due to variations in the added mass. A region of positive C_{lv}, for example, shows the region where net energy is transferred from the fluid to the structure, effectively providing excitation where vibration of the structure may occur. This measurement from forced motions can be used to predict the motions of an elastically mounted cylinder, as in Staubli (1983), or in the more complex semi-empirical prediction of VIV of long, slender, continuously flexible structures in shear flow (Zheng et al., 2014b). While an initial measure of the interaction between sinusoidal cylinder motions and the resulting hydrodynamic forces acting on the body, portions of the parameter space were fairly coarse in measurements and the parameter space was limited in Reynolds number.

Additional forced motion experiments have been conducted for similar problems of a cylinder encountering a free stream and forced to move with prescribed sinusoidal motion perpendicular to the flow direction. A series of experiments were conducted by Vikestad et al. (2000) in a tow tank, similar to Gopalkrishnan (1993), for higher Reynolds numbers, showing some of the variation in measured forces due to Reynolds number.

In order to predict response and wake modes for elastically mounted circular cylinders in a fluid flow, Morse and Williamson (2009a) employed controlled-vibration experiments, which comprised of prescribed CF motion of a cylinder in the flow, over a wide regime of amplitude and frequency. Very fine adjustments of amplitude and frequency were made to perform in excess of 5000 experiments for a given Reynolds number, providing very fine resolution of the variation in forces as a function of cylinder kinematics. In addition, the experimental set was repeated three times at different Reynolds numbers in order to demonstrate variations in forces due to an increase in Reynolds number. One finding from this extensive study was the importance of fine resolution experiments to identify certain phenomena, such as an overlapping branch region of the wake, where a hysteretic wake response can occur and unique wake modes are observed. It was found that for some combinations of non-dimensional amplitude and frequency, multiple wake responses were possible and these different responses were observed when the recirculating water channel underwent either an increase or a decrease in flow speed (Morse and Williamson, 2009b). In this overlapping hysteretic region, distinct vortex modes were identified through quantitative flow visualization.

These forced motion studies have shown the complex forcing on a circular cylinder due to vortex shedding in the wake, but recent studies have shown how this forcing can change when the cylinder is free to move in only the IL direction or with a combined IL and CF motion. A series of recent studies have characterized the behavior of forcing and mode formation for a cylinder undergoing pure IL motion. For example, Cagney and Balabani (2013a) evaluated the motion and velocity field of an elastically mounted cylinder undergoing VIV in pure IL motions. It was observed that hysteresis and multiple wake modes occur in the region of the second response branch. Additionally, they observed three overlapping branches at the same reduced velocity, with different vortex patterns corresponding to each branch. Multiple response branches were also observed in Gurian et al. (2019), appearing to be a feature of streamwise oscillation. Previous studies have also characterized interesting response features of pure IL motion vibrations including alternating and symmetric wake modes (Cagney and Balabani, 2013b; Konstantinidis, 2014) and the unusual response characteristics as a result of drag force effects (Cagney and Balabani, 2016).

In the case of combined IL and CF motion, the combination of exciting multiple directions of motion results in additional complexity to conducting experiments and understanding the wake and forces. Sarpkaya (1995) performed a set of free vibration tests using an elastically mounted cylinder subject to an incoming flow on a spring system that could be configured to have equal or 2:1 ratio of IL:CF natural frequencies. When the cylinder can move with combined IL and CF motion, CF oscillations are larger than when it can only move perpendicular to the flow (CF). This study found a unique double peak response with the 2:1 ratio of natural

frequencies. The comprehensive experiments of Jauvtis and Williamson (2004) on a cylinder with equal mass ratio in both IL and CF direction along with equal natural frequency in each direction demonstrated very large CF motions (in excess of 1.3 cylinder diameters), and this large motion was shown to be associated with a wake mode consisting of two vortex triplets shed each cycle, denoted as the '2*T*' wake mode. Additionally, for some force conditions, a significant third harmonic component of force was noted. Through a series of free vibration experiments Dahl et al. (2006, 2007) and Dahl et al. (2010), it was demonstrated that for various IL to CF natural frequency ratios, a significant third harmonic force component, resulting from the relative motion of the body with respect to vortex shedding, can become dominant with a magnitude greater than the first harmonic component of force, indicating conditions with significantly different forcing than those observed for a cylinder oscillating only perpendicular to the flow direct. In these conditions, linear approximations of the force would be insufficient at capturing these force components, which can have a significant effect on the fatigue life of structures (Mukundan et al., 2009). Cagney and Balabani (2014) made direct comparisons between the wake mode generation of a pure IL excitation and combined IL and CF excitation was, finding that the addition of CF motion limits the system response to one branch.

While the response of cylinder VIV in combined CF and IL motion has been investigated in several studies through free vibration experiments, few studies have investigated the forces on a cylinder through forced motion experiments, which can be used for developing predictive models. An initial set of forced motion experiments was performed by Jeon and Gharib (2001), where a limited set of forced motion two-degree-of-freedom (2-DOF) experiments were performed. In these experiments, the amplitude of motion in the IL and CF directions were fixed and the phasing between these motions was investigated for two cases. The resulting wake mode was shown to be associated with this phase between motions, where it was concluded that the CF motion of the body controls the vortex shedding process, while the IL motion sets the relative phase of vortex shedding. This set of experiments, however, only covered a very small subset of possible motions that a body may undergo in VIV excited in 2-DOF. Aronsen (2007) performed a small set of forced motion experiments, including pure IL and combined IL and CF forced motion experiments, and discovered that it may be possible to predict the motions of a long, flexible cylindrical structure using such a force database if the database is sufficiently resolved, but this study focused primarily on small scale motions over a very limited parameter space.

A more extensive set of forced motion experiments were conducted by Dahl (2008) in a small towing tank by parameterizing the motion of the cylinder as sinusoidal in both the IL and CF directions. This database provided an initial measurement of the forces associated with combined IL and CF motion in a free stream, demonstrating the wide range in effective added mass in both directions, as well as how IL motion and phasing can influence the prominence of higher force harmonics in lift. However, one shortcoming of this database was the coarseness of measurements. With four parameters driving the cylinder's motion (IL and CF amplitudes, CF reduced velocity and phase angle between IL and CF motions), each parameter was only varied 6–8 times, resulting in an extremely coarse interpolation of forces over the study parameter space. This data set was expanded by Zheng et al. (2014a) by performing an additional set of forced motion experiments, focusing on a range of smaller IL amplitudes and additional phases between IL and CF motions. When combined with the experiments from Dahl (2008), this database was used for initial prediction of a flexible riser undergoing combined IL and CF motions. Even with the addition of experiments of Zheng et al. (2014a), the database was still considerably coarse compared to previous forced motion experiments for purely CF motion, such as Gopalkrishnan (1993) or Morse and Williamson (2009b).

Bearman (2009) discusses how Morse and Williamson (2009b)'s highly resolved data-set allows for an in-depth understanding of the physics in the fluid–structure interaction for a cylinder undergoing a single degree of freedom VIV excitation, highlighting the necessity for this type of study to be extended to the combined IL and CF problem. Coupled forces and motions from VIV must be considered when predicting combined IL and CF motion and developing force models for these complex wakes. The curse of dimensionality, which increases the required experimental data space exponentially as the number of experimental variables increases, is one of the key obstacles with expanding forced motion studies. Consider Morse and Williamson (2009b)'s high resolution forced motion study, which altered only two motion parameters while maintaining the Reynolds number constant. When the total number of experimental runs for a given Reynolds Number (5680) is divided by the number of parameters, an effective resolution of 75.4 is obtained (effectively each parameter is varied 75 times). This is not an exact measure of each parameter's resolution, but it provides a reasonable estimate of database resolution for comparison with similar experiments. When compared to Gopalkrishnan (1993), the effective resolution was 17.5, which was much lower than Morse and Williamson (2009b) but still more than adequate for defining forces from the parameterized data space. As the number of variables required to cover a parameter space grows, so does the resolution. Table 1 compares the number of experiments and effective resolution for the aforementioned single degree of freedom forced motion experiments to the two degree of freedom forced motion research from Dahl (2008), Zheng et al. (2014a). In those cases, the resolution of experiments is much lower due to the increase of motion parameters from 2 to 4, but one can see that when increasing the number of experimental variables from 2 to 4, in order to maintain an equivalent evenly spaced resolution to Gopalkrishnan (1993), nearly 94,000 experiments are required, and in order to achieve an equivalent resolution to Morse and Williamson (2009b), 32,321,000 experiments are required.

While some recent studies have attempted to address the curse of dimensionality through automated experimentation with adaptive sampling techniques, as in Fan et al. (2019b,a), which can then be applied for prediction as in Fan et al. (2019c), the process of conducting physical experiments is still time consuming and some features of strongly non-linear processes can be difficult to discern from specific types of experiments. For example, hysteretic behaviors in VIV can be attributed to blockage and mass ratio effects (Prasanth et al., 2011), however these effects are sometimes difficult to discern in towing tank experiments as opposed to recirculating flow channel experiments, due to the stop/start nature of the experiments. In the present study, instead of focusing on techniques to reduce the parameter space, we take a simple approach to focus on increased parameter resolution on two parameters of interest, while leaving a coarse resolution on other parameters. In particular, we use a high resolution parameter space in reduced

Table 1
Previous one degree of freedom controlled motion experiments showing equivalent resolution to two degree of freedom controlled experiments; Previous and current resolution of two degree of freedom controlled motion experiment.

Experiment (1-DOF)	Runs	Resolution	Equivalent 2-DOF runs
Gopalkrishnan (1993)	306	17.5	93,800
Morse and Williamson (2009)	5680	75.4	32,321,000
Experiment (2-DOF)			
Dahl (2007)	2304	6.9	2304
Zheng (2014)	3402	7.6	3402
Present Study	9555	9.9	9555

velocity, a medium resolution parameter space in phase between IL and CF motions, and a coarse parameter space in motion amplitude. While this method is not flawless, we demonstrate that interesting new physics may be observed, observing branched wake regions where multiple possible wakes and force coefficients for the cylinder exist for a given set of motion parameters, even while performing experiments using a towing tank setup. These observations are possible simply based on the increased resolution of the reduced velocity parameter and the repeatability of an automated robotic experimental system. Additionally, we demonstrate through flow visualization that this branched wake region corresponds to mode changes in the wake, particularly changes in the dynamics of co-rotating pairs of vortices.

2. Experimental methods

2.1. Controlled motion experiments

When a system undergoes 2-DOF VIV, the resulting motions, when viewed in a carriage-fixed coordinate system, can result in figure-eight and crescent shape motions of the cylinder (Jauvtis and Williamson, 2004), which are consistent with the excitation of a system where the IL excitation has twice the frequency of the CF excitation. In some instances, it is possible for the IL excitation of the system to be excited at the same frequency as the CF direction, which can result in tear drop shaped orbital motion of the cylinder (Kang and Jia, 2013; Srinil et al., 2013; Gedikli and Dahl, 2017; Gedikli et al., 2018), however these motions are less prevalent in the vibration of engineered structures. Due to the non-linear interaction of the structural system with the fluid, there is no guarantee that these motions are sinusoidal in each direction, however, sinusoidal motions can approximate these responses to first order. To limit the parameterization of a system undergoing forced motion, we use motion definitions for a cylinder undergoing combined IL and CF excitation as given in Jauvtis and Williamson (2004), Dahl et al. (2006). The motion of the body in the IL and CF directions is assumed to be sinusoidal, such that these motions are only defined by a single amplitude and single frequency, effectively truncating a Fourier series of the cylinder motion. The IL motion is assumed to have twice the frequency of the CF motion, consistent with observations of a large number of freely vibrating systems undergoing VIV (Sarpkaya, 1995; Jauvtis and Williamson, 2004; Dahl et al., 2006). Additional parameterization of cylinder motion to include non-linear motion and additional frequency components would likely require more selective experimental techniques, such as those described in Fan et al. (2019c,b). The forced motion of the cylinder in a frame fixed to a moving carriage can then be defined as forced motion perpendicular to the flow direction (y) and forced motion IL with the flow direction (x):

$$y = A_y sin(\omega t) \tag{1}$$

$$x = A_x sin(2\omega t + \theta) \tag{2}$$

where A_x represents IL amplitude response, A_y represents CF amplitude response, ω is the angular frequency of motion.

The phase difference between IL and CF motions, θ, defines the orbital motion of the cylinder in the carriage fixed reference frame. Fig. 1 illustrates how this orbital motion of the cylinder changes as a function of the phase angle. In this figure, the flow velocity is assumed to be left to right, such that a 0° phase corresponds to a figure eight motion where the cylinder in moving upstream at the extents of the motion. Dahl et al. (2007) referred to this type of motion as counterclockwise(CCW), since the top portion of the figure eight is moving in a counterclockwise motion. Consequently, a 180° phase corresponds to a figure eight motion in the opposite direction and is designated as clockwise (CW) according to the definition used by Dahl et al. (2007).

Normalizing the frequency of motion, we define the reduced velocity based on the CF frequency as:

$$V_r = \frac{2\pi U}{\omega_y D} \tag{3}$$

It is important to note here that in contrast to a freely vibrating system, a system undergoing forced motion does not have a natural frequency, hence the reduced velocity is defined according to the frequency of vibration. To make a direct comparison between a system undergoing forced motion and a freely vibrating system, one must define the reduced velocity in the freely vibrating system based on its observed vibration frequency, as described in Moe and Wu (1990).

Additionally, we normalize the amplitude of motion in the IL and CF directions by the cylinder diameter:

$$A_y^* = \frac{A_y}{D} \qquad A_x^* = \frac{A_x}{D} \tag{4}$$

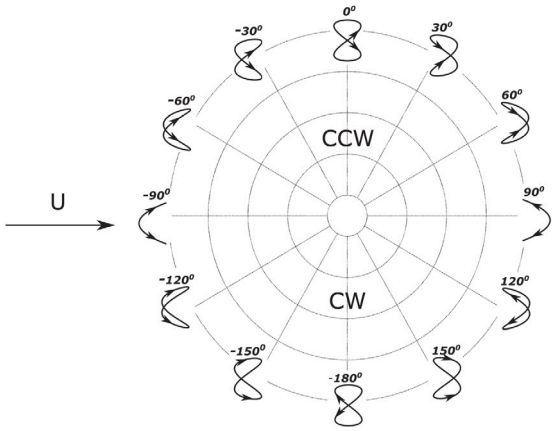

Fig. 1. Definition of the variation of phase between IL and CF motion, θ in degrees. The upper portion of the polar plot is designated as counterclockwise(CCW) and lower portion is designated as clockwise motion (CW) according to the definition used by Dahl et al. (2007). Flow velocity is left to right.

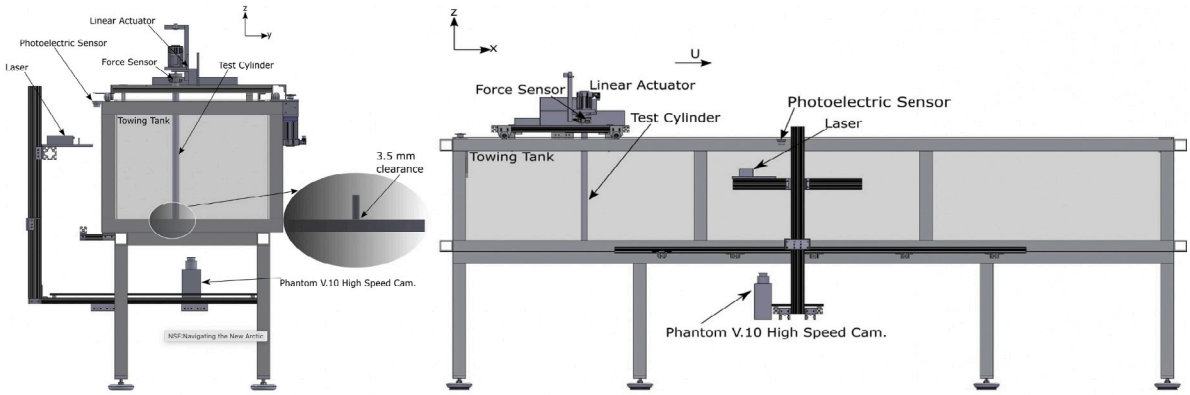

Fig. 2. Schematic drawing of the experimental setup (left image: end view, right image: side view). Controlled motion of the test cylinder is performed in the x–y plane.

The forced motion of the cylinder can then be parameterized according to four non-dimensional parameters: A_y^*, A_x^*, θ, and V_r for a constant Reynolds number.

Forced motion experiments were conducted where a circular cylinder (D = 3.85 cm, submerged length, L = 57.25 cm, m = 0.2679 kg) is towed down the length of a small tank at constant forward speed and forced to move with prescribed sinusoidal motion as defined by the above parameterization. The experiments were conducted in a small flow visualization tank that is 107 cm wide, 400 cm long, and 75 cm deep. All tests were conducted with the same forward speed, such that Reynolds number based on the cylinder diameter is the same with a value of 7620 for all experiments. The tank was equipped with a motorized tow carriage and x–y actuator system, allowing the cylinder model to be towed with a constant speed and undergo the precision forced motion. The carriage and motor system were computer controlled, enabling highly repeatable and automated experiments, also enabling a large number of experiments to be conducted. Hydrodynamic forces were measured using ATI Gamma SI-65-5 and SI-130-10 six-axis force sensors with resolution of respectively $1/80$ [N] and $1/40$ [N] in x and y directions. To maximize sensor resolution for given prescribed motions, two separate sensors were used, with the larger range sensor used for larger forced motions. The non-dimensional parameters governing the motion of the body were varied in the following format: 1) IL amplitude varied from 0.1 to 0.5 in increments of 0.1, 2) the CF amplitude varied from 0.1 to 1.6 in increments of 0.25, 3) the reduced velocity varied from 4 to 8 in increments of 0.2 and 4) the phase between IL and CF motions varied from $-180°$ to $180°$ in increments of $30°$. While $-180°$ and $180°$ represent the same motion, these runs were performed to provide a subsample of repeated experiments in the dataset. Ultimately, a total of 9555 experiments were performed. Fig. 2 shows a schematic drawing of the experimental setup, illustrating the location of the force sensor and definition of the coordinate system. A summary of the test apparatus parameters is given in Table 2.

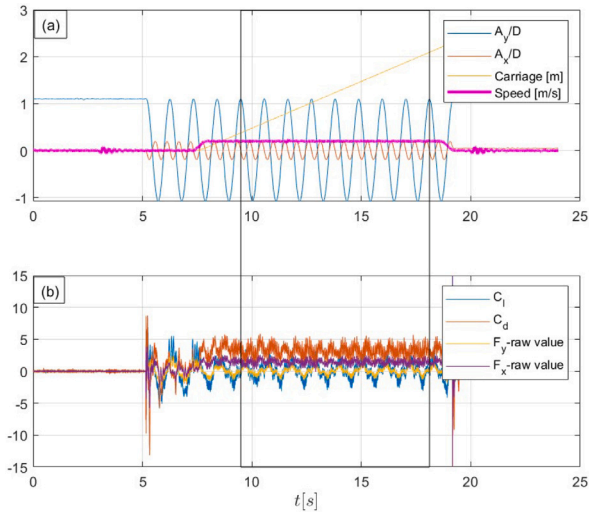

Fig. 3. Time trace of motion region showing non-dimensional cross flow and IL motion amplitude, carriage distance, carriage speed in (a), lift and drag force coefficients and the force signals before subtracting the inertial force in (b) for an example run: $A_y/D = 1.1$, $A_x/D = 0.2$, $V_r = 5.6$, $\theta = 0°$.

Table 2
Experimental model parameters for controlled motion experiments.

Experimental parameters	Values
Diameter, D	3.85 cm
Submerged Length, L	57.25 cm
Towing speed, U	0.2 m/s
Reynolds number, Re	7620

2.2. Hydrodynamic force decomposition

Since the force sensor attached to the test cylinder measures both the hydrodynamic force and the inertial force of the test cylinder, the inertial force is subtracted from all measurements in order to report only the hydrodynamic force. The inertial force is determined based on the measured acceleration of the cylinder, using motor encoder positions and the measured mass of the cylinder. The hydrodynamic force is then decomposed as a force acting in the direction of the mean flow (drag, F_x) and a force acting perpendicular to the direction of the mean flow (lift, F_y). These hydrodynamic forces are normalized using typical lift (C_l) and drag (C_d) force coefficient definitions scaled by the density of the water, ρ, flow speed, U, cylinder diameter, D, and submerged cylinder length L:

$$C_l = \frac{F_y}{\frac{1}{2}\rho U^2 DL} \quad , \quad C_d = \frac{F_x}{\frac{1}{2}\rho U^2 DL} \tag{5}$$

For each parameter combination, a time history of force and motion is measured. Fig. 3 shows an example of the non dimensional CF and IL motion amplitude, carriage travel distance, carriage speed, and raw force measurements. For force calculations, we clip the force data after the carriage has reached a steady state forward speed and transients in the lift force are no longer observably present. In the example time histories shown in Fig. 3, this trimming occurs for the fourth cycle of motion in the CF direction. Fig. 4 shows an example processed time history of measurements for a specific run, illustrating the normalized motion in the CF and IL directions along with the measured and filtered normalized lift and drag force. As shown in the time history, the cylinder is initially allowed to oscillate for at least three cycles while stationary before the carriage begins to tow the cylinder with a forward speed. As opposed to a freely vibrating cylinder being towed forward, where many cycles of vortex shedding may be necessary to establish synchronization of the wake with the structural system, synchronization of the wake can occur much more quickly, with fewer cycles of motion (Peppa et al., 2021). The initial motion of the body in the present experiments before towing allows for rapid synchronization as the body is then towed forward, as observed through matching of the dominant hydrodynamic force frequency with the motion frequency. As seen in Figs. 3 and 4, the forced motion quickly results in time dependent forces synchronizing with the motion of the body. While there is some slight natural variation from cycle to cycle, the cyclical forces are highly repeatable. It should be noted that this experimental process is not perfect and the length of the current experimental tank does pose limitations on the experiment. In particular, we limit V_r to a maximum value of 8 since the number of cycles that can be performed over the length of the tank becomes very small as reduced velocity increases. We show later through validation of the experimental apparatus, that this limitation does not have a significant impact on the measurement of hydrodynamic forces and the development of dynamic equilibrium in the wake for the vast majority of experiments performed in the present study.

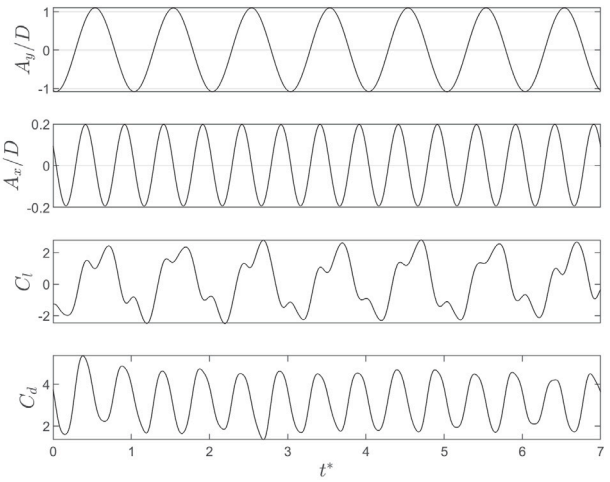

Fig. 4. Time trace of CF and IL motion and time dependent lift and drag force for an example run: $A_y/D = 1.1$, $A_x/D = 0.2$, $V_r = 5.6$, $\theta = 0°$.

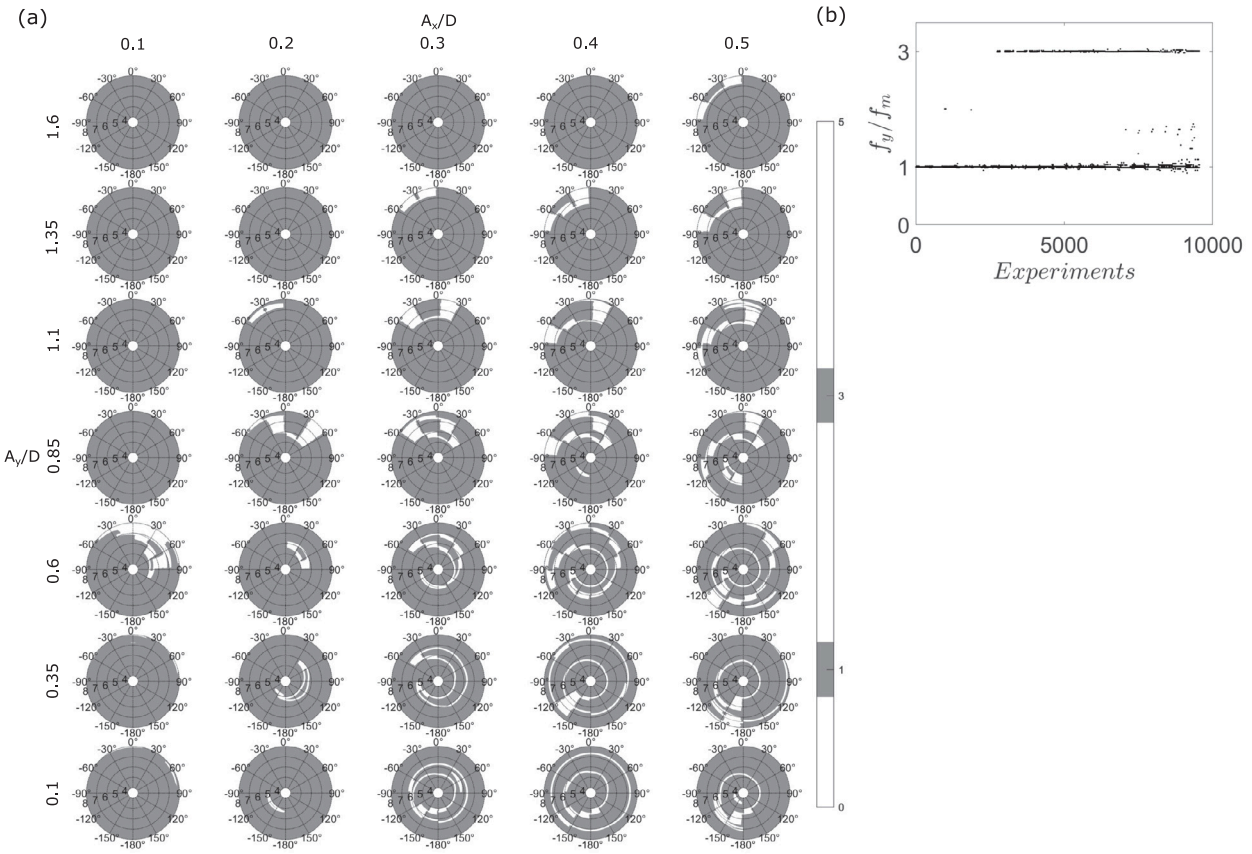

Fig. 5. Peak frequency analysis from power spectrum density based on lift force coefficient as a function of four parameters: V_r, θ, A_x/D, A_y/D. Left image (a) shows the x-axis shows variation of non-dimensional IL amplitudes, $A_x/D = 0.1$, 0.2, 0.3, 0.4, 0.5. The y-axis shows variation of non-dimensional CF amplitudes, $A_y/D = 0.1$, 0.35, 0.6, 0.85, 1.1, 1.35, 1.6. Right image (b) shows Frequency ratios in CF.

To illustrate synchronization of the wake with the body motion, Fig. 5 shows the dominant frequency of the hydrodynamic force in the CF direction normalized by the motion frequency for all performed experiments (experiment number is shown on the x-axis of the subfigure to the right). One can see that the vast majority of experiments demonstrate a dominant lift frequency equal to or very near the motion frequency, or equal to three times the motion frequency. This indicates synchronization of the wake with

the body motion for the majority of experiments, knowing that some motions can produce a dominant third harmonic force (Dahl et al., 2007). In the left portion of the figure, polar plots help to illustrate synchronization in the data set visually, where each polar plot is drawn for a fixed combination of A_y/D and A_x/D with variation of the phase between motions, θ as the angle of the plot and variation of reduced velocity along the rays. The white regions indicate areas where the first or third harmonic of force was not the dominant frequency component in lift. It should be noted, however, that this does not in itself, rule out synchronization of the wake with motion, as all of these cases had significant frequency components equal to the motion of the body and the mode of the wake should be considered in any analysis of the dominant frequencies as well. In particular, a frequency doubling mode formation, such as the alternating-symmetric mode observed in pure IL experiments (Gurian et al., 2019), could result in significant even harmonics or half frequencies (e.g. $f_y/f_m = 1.5$ or 2). For brevity, this current paper focuses primarily on an analysis of specific observations from forces related to branches and the resulting wakes, while a subsequent paper will investigate wake formations more generally from this experimental data set.

Because the hydrodynamic forces acting on the cylinder are a function of the cylinder's relative motion with respect to vortices shed in its wake, it is necessary to decompose the hydrodynamic forces into excitation forces in phase with the velocity and excitation forces in phase with the acceleration of the body to understand how these forces interact with the body dynamics as in Sarpkaya (2010). These components of the force are directly proportional to the added damping and added mass of freely vibrating systems. Although these forces are not perfectly sinusoidal in reality, decomposing them into forces in phase with acceleration and velocity allows one to evaluate the effective excitation and change in the effective added mass of a freely vibrating system to leading order. While higher harmonic forcing is known to be enhanced by combined CF and IL motion, for brevity, we focus on the leading order force terms in this study. To be noted, since the forced motion frequency is only a single frequency, any higher frequency noise or higher frequency components from vortex shedding will not contribute to the added mass and added damping as computed from the in phase components of the force. This does not mean that forcing frequencies that are different from the body motion frequency could not have an effect on the added mass of a freely vibrating system undergoing non-sinusoidal motion, but that effect is not measurable from the force measurements alone in the present experiment, since the body motion does not contain any higher frequency components.

If one assumes a 1-DOF sinusoidal body motion and a phase shifted forcing function of the form

$$F_l = F\sin(\omega t + \phi) \tag{6}$$

as in Williamson and Govardhan (2004), then through trigonometric expansion, the portion of the force in phase with velocity is

$$F_{lv} = F\sin(\phi) \tag{7}$$

and the portion in phase with acceleration is

$$F_{la} = F\cos(\phi) \tag{8}$$

where F_l represents the lift force, F_{lv} represents the lift force in phase with velocity, and F_{la} represents the lift force in phase with acceleration. When normalized as a lift or drag coefficient, these forces can be expressed as the lift coefficient in phase with velocity, C_{lv}, and the lift coefficient in phase with acceleration, C_{la}. As described in Smogeli (2002), these quantities may be decomposed by evaluating the inner product between the lift coefficient time history and the motion time history (either in phase with velocity or acceleration depending on the relevant coefficient). For a sinusoidal function, the inner product (performed inside the sum from Eq. (9)) is mathematically equivalent to the expressions in Eqs. (7) or (8). This process can be performed over an individual cycle of motion to obtain the lift in phase with velocity for a single cycle and averaged over N observed cycles. The resulting coefficient is a single value that represents a cycle averaged magnitude of the portion of lift in phase with velocity or acceleration as shown in Eqs. (9) and (10), where the subscript i denotes a single cycle within the time history of N cycles.

$$C_{lv} = \frac{1}{N}\sum_{i=1}^{N}\sqrt{\frac{2}{T_i}}\frac{\langle C_{li}(t), \dot{y}_i(t)\rangle}{\sqrt{\langle \dot{y}_i(t), \dot{y}_i(t)\rangle}} \tag{9}$$

$$C_{la} = \frac{1}{N}\sum_{i=1}^{N}\sqrt{\frac{2}{T_i}}\frac{\langle C_{li}(t), \ddot{y}_i(t)\rangle}{\sqrt{\langle \ddot{y}_i(t), \ddot{y}_i(t)\rangle}} \tag{10}$$

The same procedure can be applied to IL motion as well to define oscillating drag coefficients C_{dv} and C_{da} with respect to the inline motion $x(t)$. These equations are omitted for brevity as they share the same form as the IL equations.

Since the force in phase with acceleration will behave equivalently as an inertial force, we can set the force in phase with acceleration equal to an added mass times the acceleration of the body in each direction. Rearranging and normalizing the added mass, we can define an effective added mass coefficient for the IL (C_{mx}) and CF (C_{my}) directions. This effective added mass contains the ideal potential flow added mass in addition to the effects of vortex formation in the wake of the cylinder. Eqs. (11) and (12) give the effective added mass coefficients for IL and CF directions. Since V_r is defined based on the CF frequency, the 2:1 relation between IL and CF frequencies results in a factor of 4 in the denominator of the IL added mass coefficient.

$$C_{my} = -\frac{C_{la}V_r^2}{2\pi^3 A_y^*} \tag{11}$$

$$C_{mx} = -\frac{C_{da}V_r^2}{8\pi^3 A_x^*} \tag{12}$$

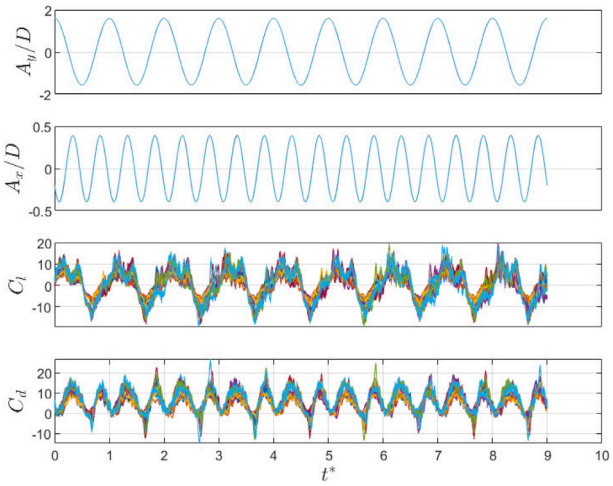

Fig. 6. Time trace of CF and IL motion and time dependent lift and drag force for an example run: $A_y/D = 1.6$, $A_x/D = 0.4$, $V_r = 5.4$, $\theta = 30°$ with repeated 20 times.

Although the IL and CF motions of the cylinder are orthogonal, the forces acting on the cylinder are a result of the same vortex shedding in the wake of the body and hence are coupled through non-linear forcing from vortex shedding. This can result in energy transfer from the IL motion of the body to CF forcing and vice versa. In the case of coupled motions, it is not sufficient to consider only excitation of the structure due to forcing in a given direction, hence the total power transfer from body to fluid over a given cycle in all motion directions can be a more appropriate measure of the coupled forcing on the structure. The average power over one cycle of motion is defined as the integral in time over one cycle of motion of the total force (including drag and lift) dotted with the velocity. The power is normalized to define an average power coefficient, C_{ap}, which can act as a representative value indicating excitation of the cylinder. A positive power coefficient indicates a system in which net energy is transferred from the fluid to the body, indicating positive structure excitation. A freely vibrating system may exhibit this type of motion. A negative power coefficient indicates a net transfer of energy from the structure to the fluid, which will only occur during forced motions or the excitation of long, flexible structures where power transfer varies along the length of the structure.

$$C_{ap} = \frac{\frac{1}{T}\int_0^T (\mathbf{F_y}\cdot\dot{\mathbf{y}} + \mathbf{F_x}\cdot\dot{\mathbf{x}})dt}{\frac{1}{2}\rho U^3 DL} \tag{13}$$

It is important to note that using the inner product to compute force coefficients does not necessarily require that the frequency of body motion be synchronized with the frequency of forcing on the body (i.e. if vortex shedding is not synchronized with cylinder motion, the forcing frequencies may differ from the oscillation frequency).

With such a large number of experiments spanning the experimental dataset and limitations to the length of the tank over which experiments were performed, it was not possible to conduct repeated experiments for every combination of parameters. In order to demonstrate that the observed forces from the experimental set are repeatable and representative of forces, one would expect to observe over a statistically significant number of cycles, an example experiment with the same input motion parameterization was performed 20 times to demonstrate repeatability. For the example reference case, we selected a large amplitude motion with a relatively low reduced velocity, which results in large magnitude forces with the potential for increased force variability and error when removing the cylinder inertial force from the measurement. Fig. 6 depicts the time histories of this motion and force from these repeated experiments, which are superimposed to visualize the variability in the raw data. The mean values of C_{lv}, C_{dv} and C_{ap} are −4.6518, −0.5908, and −4.5258 respectively for the repeated experiments (values are computed for each cycle and averaged across all cycles from all runs). The variances of C_{lv}, C_{dv} and C_{ap} are 0.0033, 0.0230, 0.0124 respectively for this experimental case, computed based on each cycles value relative to the mean over all runs. As can be seen, there is almost no variability in the measured motion of the body. While there is some variability in the measured raw forces, it is quite small. When the variance of cycles for individual runs is compared to the reported variances for all runs, there is no significant difference, demonstrating that the experiments are highly repeatable. It is impractical to repeat every experiment in this manner with a large number of experiments, however the experimental set does include repeated experiments where all phases with 180° are repeated once, such that measurement repeatability can be observed across experiments with different motion parameters. This is key as interesting cases occur where repeated experiments demonstrate different force measurements according to different response branches at this phase.

One concern about conducting experiments with a limited tank length is that the wake will have insufficient time to develop into a dynamic equilibrium. In addition to the repeated experiment described above, if we simply look at the value of the hydrodynamic coefficients, such as C_{lv}, computed on a cycle by cycle basis for any given run in the database; for the vast majority of the database,

Table 3
Comparison of force coefficient measurements for one degree of freedom forced motions with Gopalkrishnan (1993). The table shows the absolute difference (ΔC) between measurements obtained with the current apparatus, labeled with subscript 'current', and measurements obtained from Gopalkrishnan (1993), labeled with subscript 'ref'. The absolute difference over the range of example cases tested, including those outside the current reduced velocity range, show very small differences in most cases, confirming that the experimental apparatus properly measures force coefficient values with servo noise present. We show absolute difference here for validation comparison since the force coefficients can have values near zero.

A_y/D	V_r	$C_{m,current}$	$C_{m,ref}$	ΔC_m	$C_{lv,current}$	$C_{lv,ref}$	ΔC_{lv}
0.2	11.8	−0.49	−0.65	0.16	−0.09	−0.08	−0.01
0.2	6.8	−1.18	−0.70	−0.48	0.23	0.20	0.03
0.2	4.7	2.59	2.50	0.09	−0.81	−0.75	−0.06
0.2	4.0	1.67	1.45	0.22	−0.19	−0.18	−0.02
0.2	3.4	1.63	1.40	0.23	−0.32	−0.25	−0.07
0.4	11.8	−0.69	−0.58	−0.11	−0.16	−0.11	−0.05
0.4	6.8	−0.50	−0.42	−0.08	0.05	0.14	−0.09
0.4	4.7	2.31	2.35	−0.04	−0.79	−1.10	0.31
0.4	4.0	1.98	1.50	0.48	−1.06	−1.10	0.04
0.4	3.4	1.75	1.40	0.35	−1.52	−1.30	−0.22
0.6	11.8	−0.55	−0.55	0.00	−0.37	−0.30	−0.07
0.6	6.8	−0.45	−0.42	−0.03	−0.20	−0.09	−0.11
0.6	4.7	2.08	1.95	0.13	−0.75	−0.11	−0.64
0.6	4.0	2.00	1.65	0.35	−1.15	−1.10	−0.05
0.6	3.4	1.79	1.50	0.29	−2.51	−2.50	−0.01
0.8	11.8	−1.05	−0.59	−0.46	−0.52	−0.45	−0.07
0.8	6.8	−0.41	−0.45	0.04	−0.54	−0.40	−0.14
0.8	4.7	1.76	1.65	0.11	−0.36	−0.30	−0.06
0.8	4.0	1.86	1.75	0.11	−1.88	−2.00	0.12
0.8	3.4	1.77	1.55	0.22	−3.63	−2.70	−0.93
1	11.8	−1.29	−0.55	−0.74	−0.82	−0.60	−0.22
1	6.8	−0.40	−0.49	0.09	−1.08	−0.90	−0.18
1	4.7	1.14	1.60	−0.46	−1.29	−1.05	−0.24
1	4.0	1.40	1.50	−0.10	−3.07	−3.00	−0.07
1	3.4	1.65	1.45	0.20	−3.79	−3.50	−0.29

there is no systematic change in the value of C_{lv} over each run. In essence, for the vast majority of experiments in this database, the hydrodynamic coefficients do not systematically increase or decrease over the course of a run, indicating the wake has reached dynamic equilibrium. In a few exceptional cases, the hydrodynamic coefficient computed for a given cycle in a particular experiment may vary slightly between cycles. However, since each experiment is conducted independently, and the mean value (computed over all cycles in the experiment) of the hydrodynamic coefficients varies smoothly across experiments, this suggests that even in cases where some variability occurs in a given experiment, the mean value of the hydrodynamic coefficient is consistent with other experiments with similar motion parameters.

In addition, a set of selected 1-DOF forced motion experiments were conducted to make a direct comparison of the experimental apparatus with Gopalkrishnan (1993). In total, 25 validation experiments were performed with A_y/D varied from 0.2 to 1 and V_r varied from 3.4 to 11.8. Note that the largest V_r value of 11.8 in the validation dataset is an extreme case for the limiting length of the towing tank that was used for the present experiments. This results in very few cycles of motion for $V_r = 11.8$, which is typically undesirable for measuring hydrodynamic force coefficients and the reason that the reported experimental database is limited to a maximum value of $V_r = 8$. However, in all cases, even with $V_r = 11.8$, a good comparison of the value of measured force coefficients was observed in the validation dataset. Table 3 shows the direct comparison of added mass coefficient and lift in phase with velocity along with the absolute difference between the current measurements and the reference values from Gopalkrishnan (1993). While some cases show slightly larger differences than others, the magnitude and sign of the experiments are the same and the larger differences are more likely attributable to regions where there are large gradients in the force cofficient dataspace, rather than experimental error in the establishment of dynamic equilibrium of the wake. This provides an additional check on the validity of computing force coefficients from the limited cycles provided in the present experimental study.

2.3. Quantitative flow visualization

To relate observations from force measurements to vortex formation in the wake, quantitative flow visualization experiments were performed on a subset of the experimental test matrix. Digital particle image velocimetry (DPIV) was used to measure the wake of the cylinder for a selected number of experiments. Time resolved 2-D DPIV was performed using a Phantom V10 high speed camera, laser with light sheet optics, seeding particles, and processed using LaVision DaVis 8 processing software. The camera and laser setup is shown in Fig. 2, where the high speed camera was located underneath the tank in order to capture images in the wake of the cylinder while the laser was positioned to shine a thin light sheet through the side window of the tank. The camera and laser were mounted to a carriage underneath the tank such that the DPIV setup followed the upper carriage motion, obtaining wake measurements in a fixed carriage reference frame. This helps with both calculation of the resulting vector field and a longer measurement of the wake in a consistent field of view, since the cylinder is confined to the same region within the camera field of view. The camera frame rate was 250 Hz. Vector fields were processed using a standard multi-level PIV algorithm starting with an interrogation window size of 64 × 64 and ending with a final window size of 32 × 32.

3. Force coefficient database

In this section, we present the measurement of fluid force coefficients observed across the experimental parameter space. Due to the fact that the parameter space consists of four independent variables and each force coefficient measurement serves as a fifth dependent variable, a single plot cannot depict the total variation of a single variable. We report the forces using polar plots that capture the variation over these parameters for a fixed combination of IL and CF amplitudes because the experiments were conducted with a higher resolution of the phase, θ, and the reduced velocity. In each polar plot, the phase lag between IL and CF motion (θ) is varied around the circumference of the plot, allowing force measurements at 180° to blend with measurements at −180°, where experiments were repeated. Reduced velocity is varied radially in the polar plot, with the lowest reduced velocities near the center of the plot and increasing radially outward. A separate polar plot is made for each IL and CF amplitude combination in order to illustrate variation of forces over the entire parameter space. For brevity, we limit the presentation of force measurements to a subset of force coefficients (C_{lv}, C_{dv}, and C_p) in order to highlight more specific interesting features of the database. We note here that this representation of the force coefficient is non-conventional as previous forced motion experiments, particularly in 1-DOF motion, typically illustrate force coefficient contours as a function of the CF amplitude and reduced velocity. Due to the discretization of the motion parameters in the current database, presenting the force coefficients in this polar plot form represents the most compact representation of the full database of measurements and helps with identifying observed multiple branch regions in the database. We selectively discuss subsets of the database using the traditional representation of this type of data in the discussion section.

3.1. Fluctuating force coefficients

Fig. 7 shows the variation of the lift coefficient in phase with velocity C_{lv} over the experimental database. C_{lv} is a measure of energy transfer from the fluid to the structure. A positive C_{lv} value corresponds with a net transfer of energy from the fluid to the structure, where excitation of the structure may occur in the CF direction. For a cylinder that is elastically mounted and free to vibrate in a uniform flow, if the cylinder oscillates with a constant amplitude, this corresponds to the C_{lv} balancing with the linear structural damping force. A system with zero structural damping would therefore correspond with contours of zero C_{lv}, and positive structural damping would correspond with positive C_{lv}. In Fig. 7, we separate positive C_{lv} values using a gray scale coloring scheme (white, gray, and black), while contours of negative C_{lv} are shown in color. Clv varies widely across the parameter space. For low CF amplitudes, the positive region of C_{lv} is almost entirely contained to the upper half of the polar plots, indicating that positive excitation can happen over a wide range of θ at low amplitudes. As IL amplitude increases, this positive excitation region moves radially outward (to higher reduced velocity). As the CF amplitude is increased, the positive excitation region again shifts radially outward to higher reduced velocities, but also squeezes into the northwest quadrant of each polar plot, indicating that positive excitation will only occur over a limited range of θ with larger amplitude motions. These observations are consistent with the phases observed in the free vibration experimental studies of Jauvtis and Williamson (2004), Dahl et al. (2007) and Dahl et al. (2010) are also consistent with observations that CCW type orbital motions (upper half of polar plot) are preferred in self-excitation of flexible structures (Gedikli and Dahl, 2017; Gedikli et al., 2018; Bourguet et al., 2011). At very high amplitude motions ($A_y^* = 1.6$), no positive excitation region is observed. This is consistent with the measured amplitudes from free vibration experiments, where CF responses were observed to be less than 1.4 diameters.

Fig. 8 shows the fluctuating drag coefficient in phase with velocity, C_{dv} as a function of the four parameters as in Fig. 7. Because large IL amplitudes are atypical of a self-excited system, C_{dv} can take on fairly large values for large IL motions greater than $A_x/D = 0.4$. To better illustrate the variability over more moderate IL motions, the contours of C_{dv} shown are restricted to values between −1 and 1. The coefficient is primarily positive for nearly all phases and reduced velocities for small IL amplitudes; however, as the IL amplitude increases from 0.1 to 0.2, specific phases between −120° and −150° become primarily negative. This shows how specific phases are unlikely to occur in the free vibration of a cylinder experiencing combined IL and CF motion, as observed in Aktosun and Dahl (2018). To understand the total response of a system undergoing combined IL and CF motions, the fluctuating C_{dv} must be considered in conjunction with C_{lv}, because energy transfer from the CF direction can still result in a negative C_{dv} even when the system is undergoing self-excitation. As CF motion amplitude increases, C_{dv} increases, becoming more positive. This indicates that an energy-in region occurs with IL motion when there are large CF motions. One may expect that for these types of motion combinations, the IL and CF directions may interact with one another, since both C_{lv} and C_{dv} can be positive in this region. As IL motion and CF motion amplitudes increase (northeast corner of Fig. 8), C_{dv} becomes largely negative, except for a small range of phases, where it is positive. In general, with increasing CF amplitude for fixed small IL amplitude, the magnitude of the fluctuating drag in phase with velocity increases, becoming more positive. However, with increasing IL amplitude for fixed small CF amplitude, C_{dv} values become more negative. One may expect then that increasing CF motion tends to enhance excitation in the IL, consistent with observations from free vibration experiments. The phase between IL and CF motion is certainly a critical parameter delineating where the sign of C_{dv} may change. An excitation region with positive C_{dv} is clearly observed between 60° and 150° for small IL motions, with the region expanding as CF motion increases.

Fig. 9 shows the average power coefficient as a function of the parameter space. Since this parameter combines excitation in the IL and CF directions, we are largely interested in delineating where C_{ap} changes sign, since a net positive C_{ap} will indicate a free body oscillation where excitation is provided by the fluid. In order to better illustrate this, Fig. 9 is plotted with two contours, colored white and gray, representing positive and negative C_{ap} values. One notable observation from C_{ap} is that the observed positive region of C_{ap}, shown in white, is overall larger than if one considered the positive region of C_{lv} by itself. This indicates that the IL motion has a net impact of increasing the excitation region of the body. In general, the positive excitation region occurs for small IL and

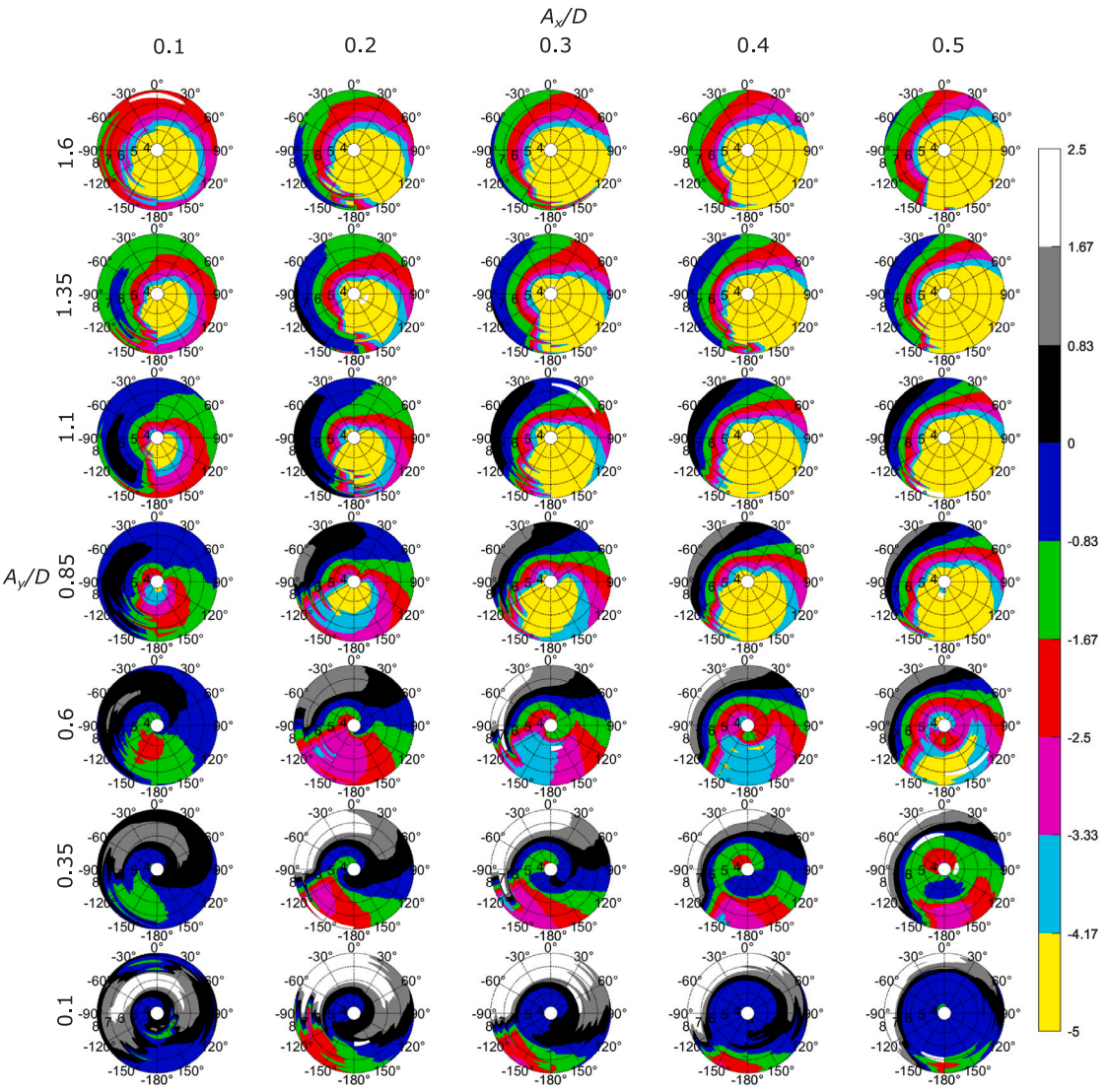

Fig. 7. Lift coefficient in phase with velocity, C_{lv}, shown as a function of reduced velocity, V_r and phase between IL and CF motion, θ for discrete combinations of IL and CF motion. The x-axis shows variation of non-dimensional IL amplitudes, $A_x/D = 0.1, 0.2, 0.3, 0.4, 0.5$. The y-axis shows variation of non-dimensional CF amplitudes, $A_y/D = 0.1, 0.35, 0.6, 0.85, 1.1, 1.35, 1.6$.

CF motions (in the southwest portion of the map). Another notable observation is that while the positive excitation region mostly corresponds with θ values associated with CCW motion of the cylinder, there are possible motions with CW phases, particularly with smaller amplitude motions.

Although contour maps of the excitation force coefficients give a global picture of the cylinder excitation forces over the parameter space, they can be difficult to comprehend in understanding force trends. To better illustrate how these forces vary for an individual combination of IL and CF amplitudes, we show variation of C_{lv}, C_{dv}, and C_{ap} for fixed $A_y/D = 0.6$ and $A_x/D = 0.1$ in Fig. 10. Each line shows the variation of the force coefficient as a function of V_r for a fixed phase θ. For most phases, the force coefficient follows a smooth trend, transitioning from negative to positive C_{lv} in many cases, or remaining negative over the entire range of V_r. However, for this particular combination of motions, one can observe that there is dramatic jumping between hydrodynamic force values for the specific phase $\theta = -120°$. For V_r between 5.8 and 7, the force coefficients fluctuate between distinctly different values, not following a smooth trend. As each data point represents the forces observed from individual experiments, this indicates some difference in the measured forces, where the measured force appears to be switching between different stable conditions. Such an observation could indicate a branched region where multiple possible stable wakes may exist. Since other phases demonstrate transitions of the force coefficient between experiments, one could reasonably conclude that the observed switching is due to a physical phenomenon. While this example figure illustrates this type of response for a fixed amplitude

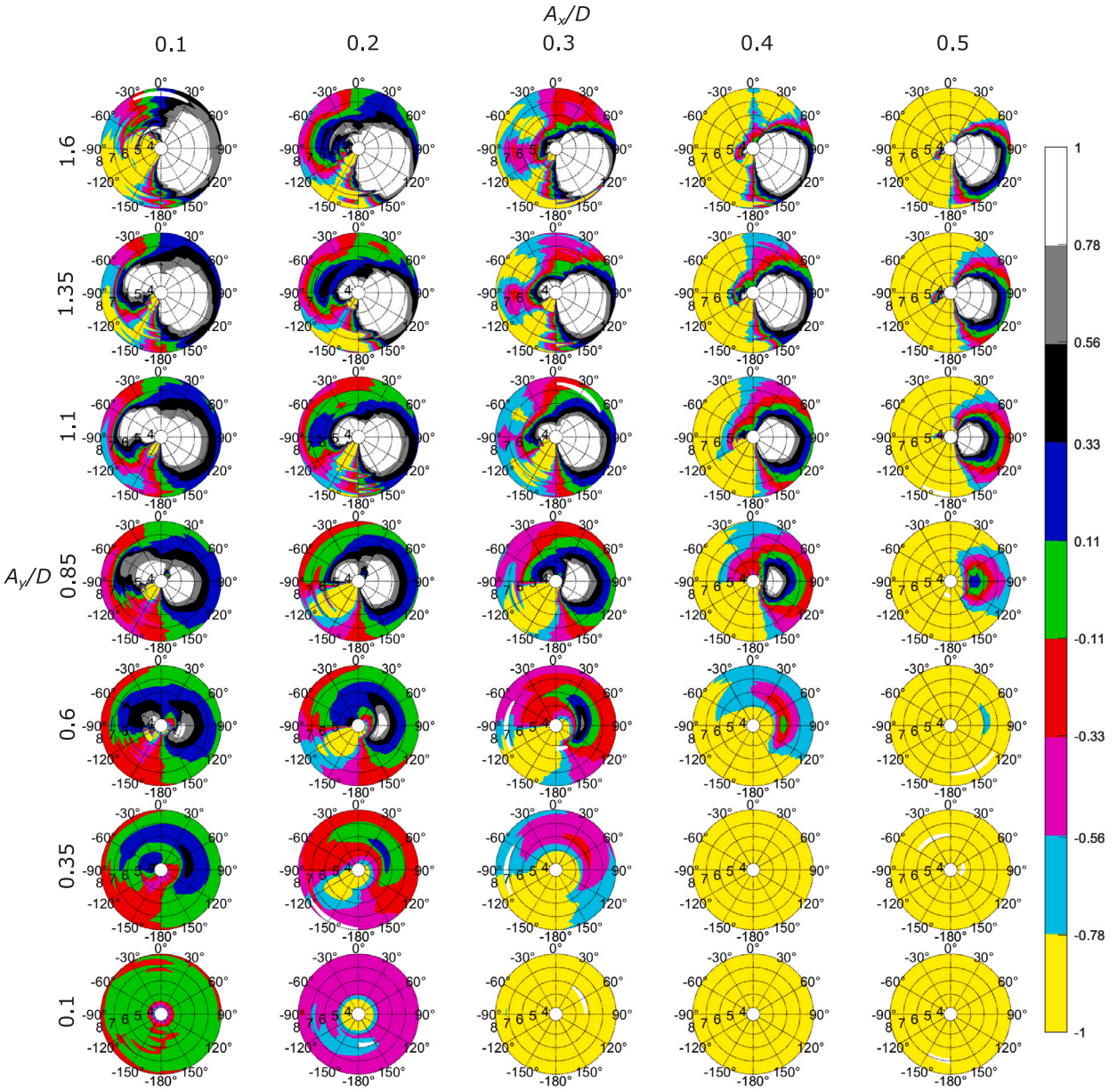

Fig. 8. Drag coefficient in phase with velocity, C_{dv}, shown as a function of reduced velocity, V_r and phase, θ between IL and CF motion. The x-axis shows variation of non-dimensional IL amplitudes, $A_x/D = 0.1, 0.2, 0.3, 0.4, 0.5$. The y-axis shows variation of non-dimensional CF amplitudes, $A_y/D = 0.1, 0.35, 0.6, 0.85, 1.1, 1.35, 1.6$.

combination, this phenomenon is observed throughout the database and investigated further in this paper through flow visualization of the wake.

3.2. Multi-branch wake regions

As seen in the example force coefficient variation in Fig. 10, for some combinations of motion parameters, significant switching between the measured hydrodynamic force values as a function of V_r was observed, which could indicate the presence of a branched wake region, where multiple possible stable wakes can exist for a given set of motion parameters. To investigate regions in the database where multiple wake branches are suspected to occur, DPIV experiments were performed over a subspace of the database to observe the resulting wake, particularly for motions where significant variation in hydrodynamic coefficients is observed. In this

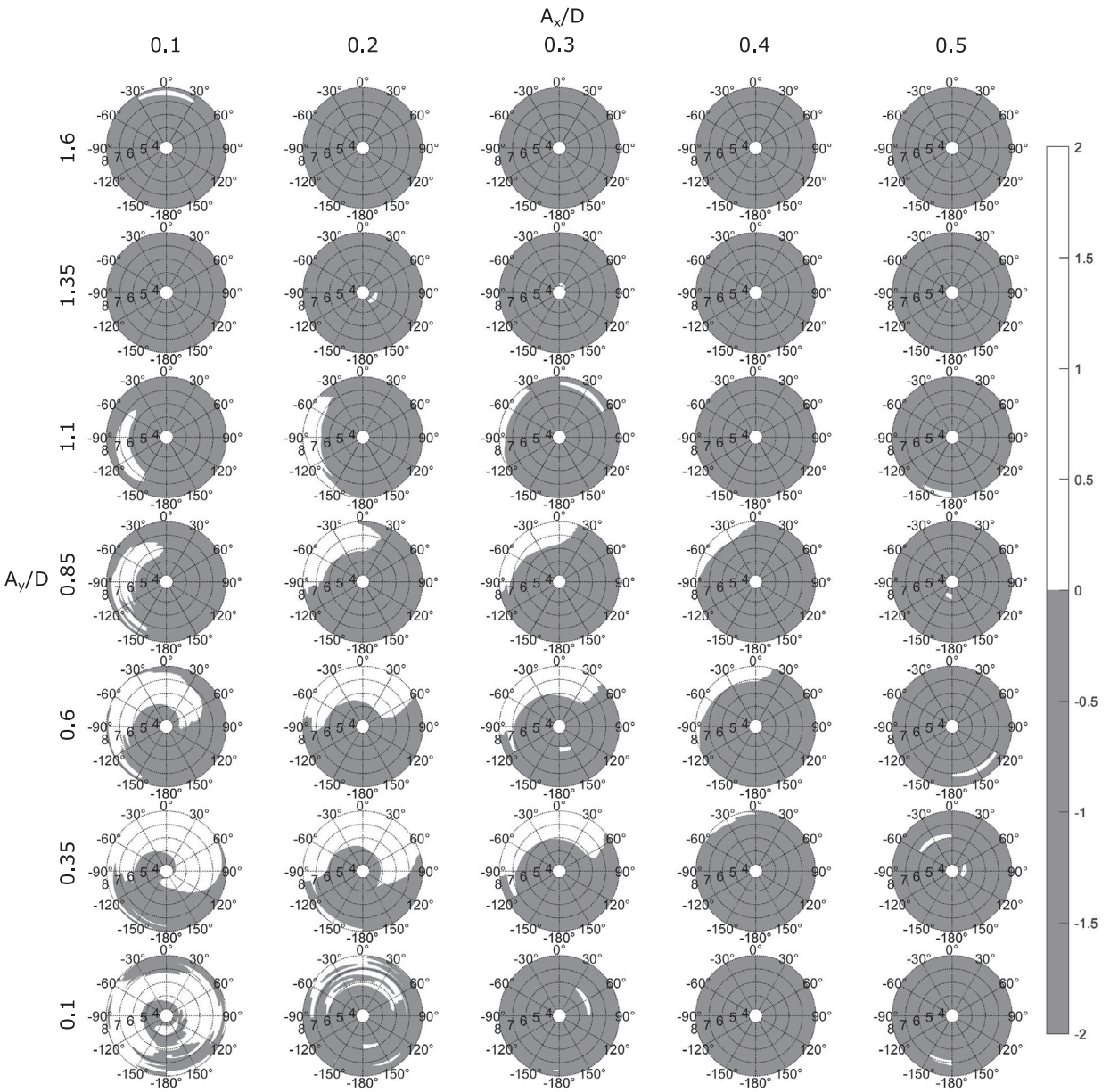

Fig. 9. Average power coefficient C_{ap} as a function of reduced velocity, V_r, phase between IL and CF motion, θ, CF amplitude and IL amplitude. The x-axis shows variation of non-dimensional IL amplitudes, $A_x/D = 0.1, 0.2, 0.3, 0.4, 0.5$. The y-axis shows variation of non-dimensional CF amplitudes, $A_y/D = 0.1, 0.35, 0.6, 0.85, 1.1, 1.35, 1.6$.

section, we identify example regions where a multiple branch response occurs as identified by variation in force coefficients, then show the time dependent wake response associated with these regions. For brevity, only two example regions are illustrated within the database, although these multiple branch regions are observed throughout the parameter space of the database.

To illustrate where a multiple branch region occurs, we first identify regions where significant fluctuations in force coefficients as a function of V_r are observed, as in Fig. 10. Since V_r has a relatively fine spacing, one would expect smooth variation of force coefficients as changes to V_r are made, hence separating individual runs into an upper branch value and lower branch value will produce two separate smooth curves for a particular force coefficient. If we separate experimental runs that demonstrate a higher force coefficient from experimental runs indicating a lower force coefficient, we can produce curves as seen in Fig. 11, which shows C_{lv}, C_{la}, and C_{my} for fixed $A_y/D = 0.6$, $A_x/D = 0.1$ and $\theta = -120°$. The separated branches clearly show the smooth variability of the force coefficients as a function of V_r on each branch. For this particular condition of motion parameters, at low reduced velocities, there is significant separation between the branches before convergence at higher reduced velocity. Here, we label the

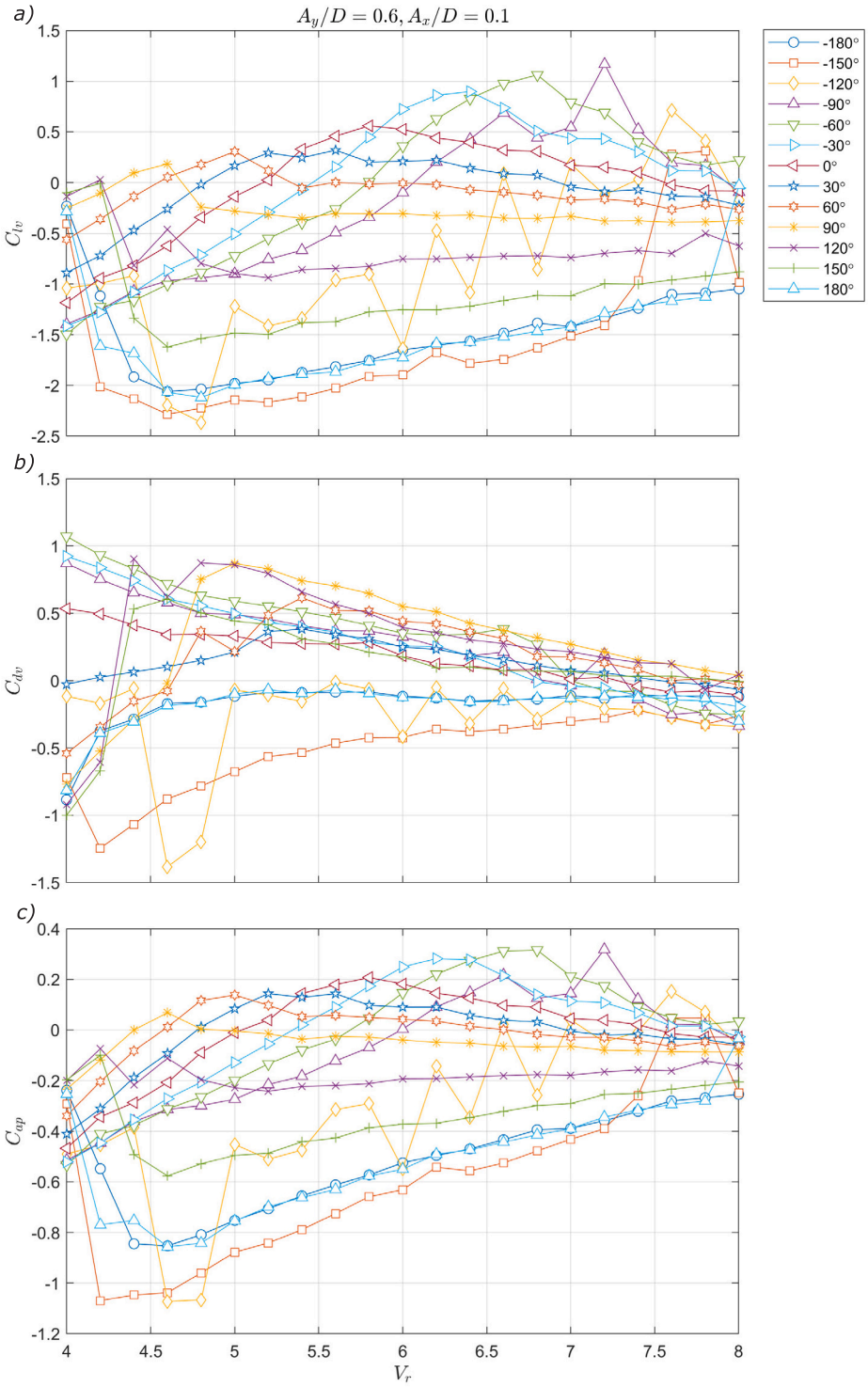

Fig. 10. Hydrodynamic coefficients for fixed $A_x/D = 0.1$ and $A_y/D = 0.6$ as a function of V_r for set phase θ. (a) Lift coefficient in-phase with velocity, C_{lv}; (b) Fluctuating drag coefficient in-phase with velocity, C_{dv}; (c) Average power coefficient, C_{ap}. Coefficients demonstrate a smooth variation over the parameter space except for $\theta = -120°$, where fluctuation in the force coefficients over a small range of $V_r = 5.8 - 7$ indicates multiple wake conditions for a fixed set of motion parameters.

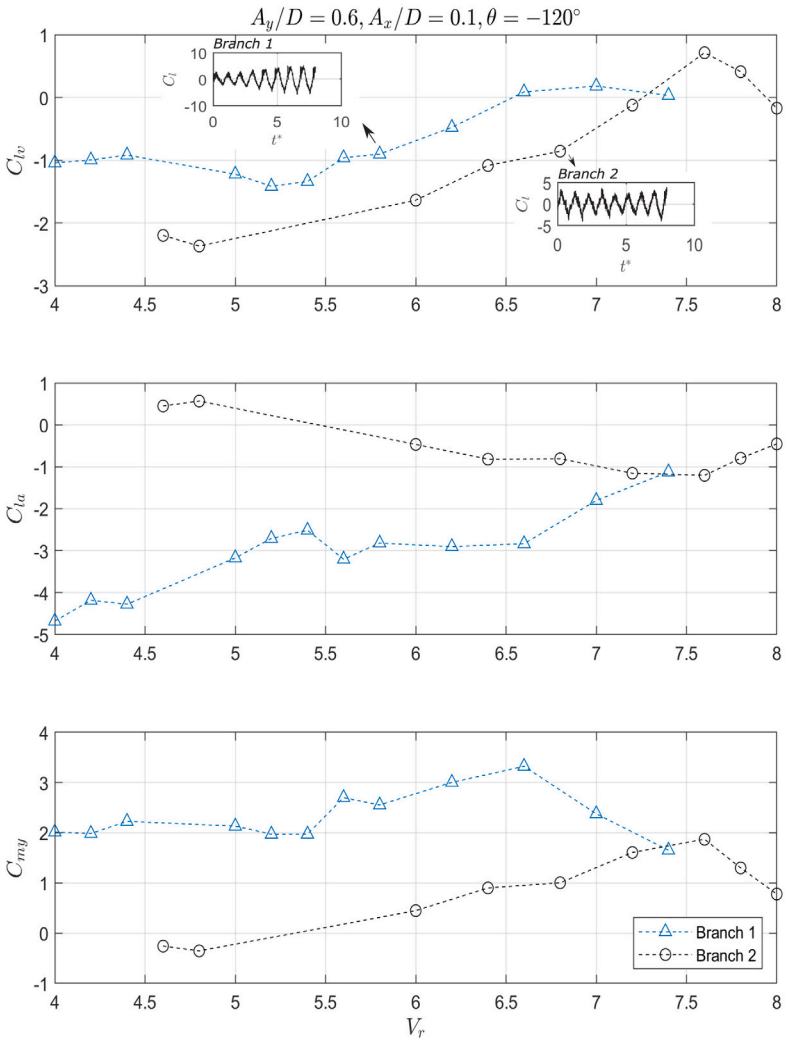

Fig. 11. Force coefficient branches observed for three hydrodynamic coefficients (C_{lv}, C_{la}, C_{my}) at $\theta = -120°$, $A_x/D = 0.1$&$A_y/D = 0.6$. Branch 1 and branch 2 correspond to different wake conditions which result in variation of the phasing between motion and forcing, force amplitude, and variation in force coefficients.

branches as Branch 1 and Branch 2 to distinguish the separate branches. Typically, hysteretic branched responses are often observed in recirculating flow channel experiments where V_r is varied by changing the flow speed in the flow channel. When a certain V_r is approached by increasing the flow speed, a certain dynamic condition may be observed, while approaching the same V_r by decreasing flow speed may yield a different observed system response. This is often difficult to observe in towing tank experiments since towing tank experiments are always started in a still fluid and any systematic bias of the experiment tends to bias the experiment to a particular dynamic response. It is significant therefore, that for very similar motion conditions, we observe both response branches, despite conducting the experiments in a towing tank.

Since the multi-branch region is not just fixed for a given θ, we must view the entire θ space for fixed IL and CF amplitude to fully see the extent of the branch region in force coefficients. Fig. 12 shows the lift coefficient in phase with acceleration, C_{la} measured over the full range of V_r and θ for fixed $A_y/D = 0.6$ and fixed $A_x/D = 0.1$. The branch region extends over a range of phases between $-90°$ and $-150°$ for this amplitude combination. The three dimensional plot of the force coefficient surface illustrates how the force coefficient region overlaps over the range of phases, such that an upper surface and lower surface exist for the same motion parameters. Several views and cutaways of the same surface are shown to better illustrate the intersection of the surfaces, where (d) shows a cutaway of the surface at the same angle θ as shown in Fig. 11. It is not surprising that particular motion combinations may result in multiple wake responses as this same phenomenon has been observed as in Morse and Williamson (2009b) for forced motion of a cylinder in pure CF motion. The interesting difference, however, is that with the increased parameter space due to the inclusion of IL forced motion, there exists a wide variety of θ and IL motion conditions that result in multiple branches of the wake and many of these regions are away from motion regions where free vibrations have been observed in previous free vibration

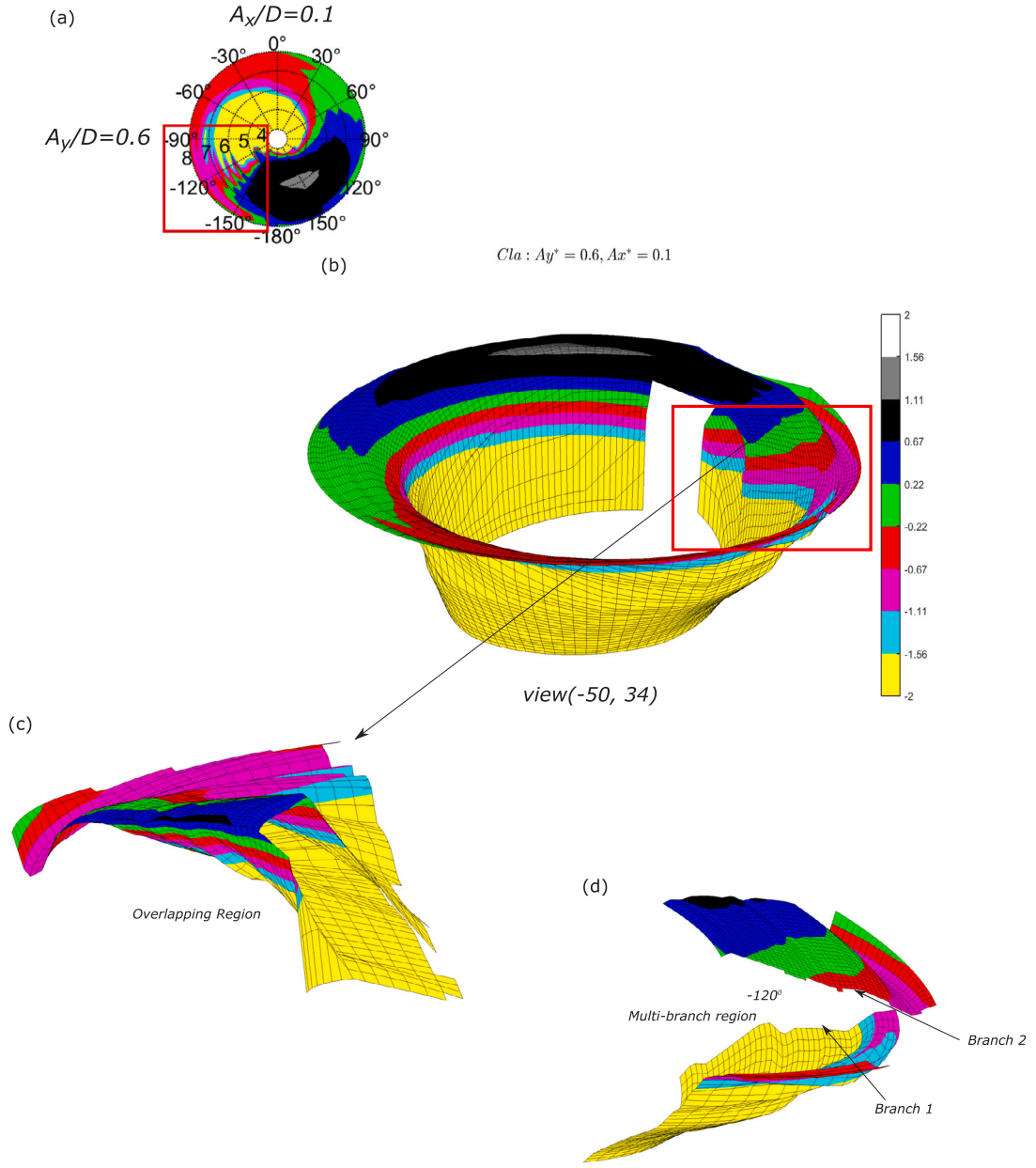

Fig. 12. Illustration of multiple branches in the polar contour plot of the lift force coefficient in phase with acceleration, C_{la}, for fixed $A_y/D = 0.6$, $A_x/D = 0.1$, and over the entire tested range of θ and V_r. Branches 1 and 2 are identified according to the same branches labeled in Fig. 11. (a) Polar plot of C_{la} for the given motion conditions, red box indicates the region where multiple branches are observed. (b) 3-D surface plot view of the same polar plot in (a) to illustrate the region where multiple branches overlap one another, the red box shows the same multiple branch region as in (a). (c) Cutaway view from backside of the overlapping multi-branch region to help illustrate the overlap.(d) Cutaway of the multi-branch region at $\theta = -120°$, edge surfaces correspond to the lines shown in Fig. 11.

experiments. To further illustrate how these branches are associated with changes to the wake, we can use flow visualization of the wake for selected experiments on each branch.

Fig. 13 shows the time history of vorticity in the wake belonging to Branch 1 (lower surface in Fig. 12) for $A_y/D = 0.6$, $A_x/D = 0.1$, $V_r = 5$ and $\theta = -120°$. Under these parametric motions, the wake exhibits periodic shedding of pairs of co-rotating vortices. Several cycles of motion are shown to better illustrate the dynamic shedding of the vortices and results are shown based on the time resolved PIV measurement, rather than phase averaged, in order to better distinguish the co-rotating vortex pairs. This pattern of vortex shedding, characterized as '2C' shedding, denoting 2 co-rotating pairs of vortices per cycle has previously been observed

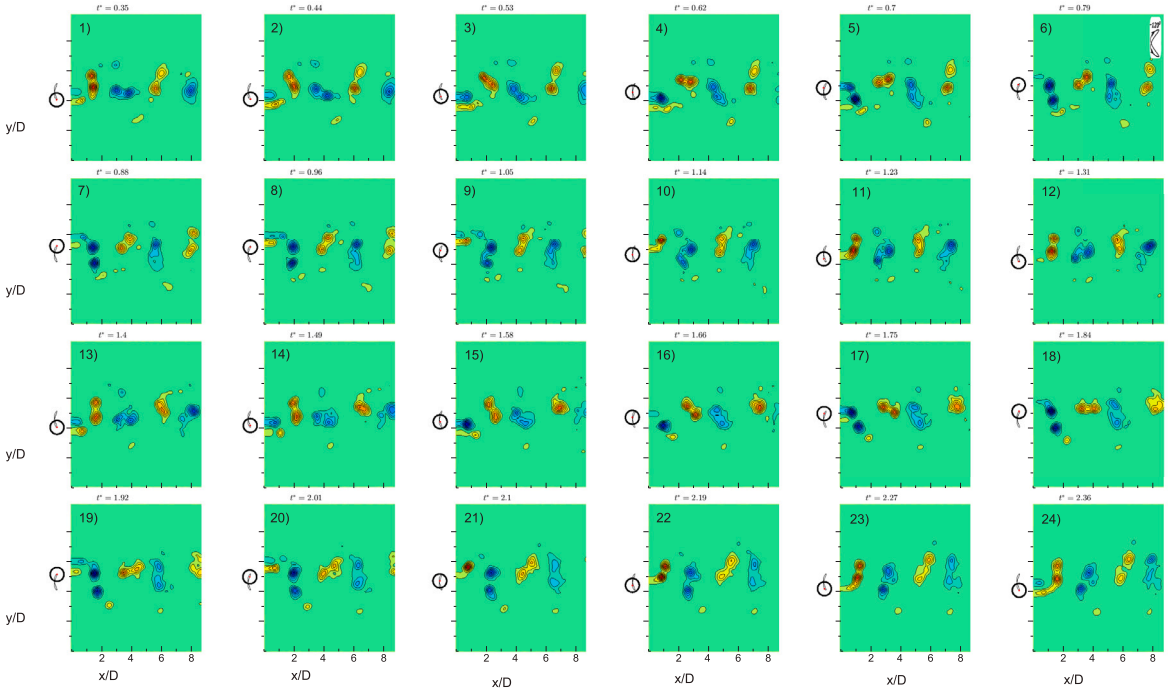

Fig. 13. Time history of wake vorticity for $A_y/D = 0.6$, $A_x/D = 0.1$, $V_r = 5$, $\theta = -120°$ corresponding to Branch 1 (lower surface of Fig. 12). Wake shows two pairs of co-rotating vortices shed per cycle, designated as '2C'. Vorticity contours show non-dimensional vorticity, $\frac{\omega D}{U}$. Supplemental Video of this wake is provided online.

in the wake of large amplitude responses observed for a pivoting cylinder as in Flemming and Williamson (2005), although it is interesting to observe this wake for fairly moderate amplitude CF motions in this case. This type of shedding pattern is very similar to the '2S' pattern, as designated as in Williamson and Roshko (1988), where two single vortices are shed per cycle of motion, since the co-rotating pair can similarly behave like a single vortex.

Since wake visualizations were performed concurrent with the original force measurements, we do not necessarily have wake visualizations for Branch 2 with the exact same V_r as Branch 1, however visualizations were obtained for slightly different V_r on Branch 2 as identified by the force coefficient analysis. Fig. 14 shows the time history of vorticity in the wake belonging to Branch 2 for $A_y/D = 0.6$ and $A_x/D = 0.1$, $V_r = 6$ and $\theta = -120°$. The wake demonstrates a '2P' type of shedding as in Williamson and Roshko (1988), where two pairs of opposite signed vortices shed from the cylinder per cycle, propagating downstream as a pair. One interesting observation from this wake is that it is very similar to the Branch 1 wake in terms of number of vortices; however, the vortices are much more spread out and separated in this wake. This separation causes the induced velocity of similar signed vortices to be significantly less. Looking carefully at the time history of the wake, one can observe that like-signed vortices actually still co-rotate in this wake, but their co-rotation is significantly less than in the Branch 1 wake, since the vortices are spread much further apart. This results in a wake that appears to follow a shape similar to '2P'. The presence of this particular branch can then be attributed to the width of the wake and spacing between vortices. Although each wake produces four vortices per cycle, Branch 1 with co-rotating vortices exhibits a wake and phasing of shedding similar to '2S', while the Branch 2 wake, with the vortices more spread out such that they propagate nearly straight downstream results in a phasing of shedding similar to '2P'.

To further quantify the variability of the wake, we observe the wake in parameter regions further away from the branch location by varying the phase between motions, θ. Fig. 15 shows a portion of the time history of the wake obtained for $A_y/D = 0.6$, $A_x/D = 0.1$, $V_r = 6$, and $\theta = -180°$. A yellow dot on the polar plot in the corner of the figure shows the location within the parameter space where the wake is observed, to the right of the multi-branch region. The wake time history in this case illustrates a similar looking wake to the '2P' Branch 2 response, which is expected since this region of the parameter space connects to Branch 2. The slight variation in θ, however, does result in a wake where one of the four vortices that are shed is slightly weaker. Due to this weaker vortex, the wake is asymmetric, where two strong vortices of alternating sign shed to the upper part of the wake, while a strong and weak vortex of alternating signs shed to the bottom part of the wake. This asymmetric wake appears very similar to a '$P + S$' type wake, although the fourth weak vortex makes it appear to be a transitional state between '2P' and '$P + S$'.

Fig. 16 shows a portion of the wake time history on the other side of the multi-branch region that connects to Branch 1. Here, $A_y/D - 0.6$, $A_x/D = 0.1$, $V_r = 6$, and $\theta = 60°$, indicated by a black dot on the polar plot in the corner of the figure. The wake demonstrates a classic '2S' shedding pattern with clear shedding of two counter-rotating vortices per cycle. Again, as this phase of motion lies away from the multi-branch region along Branch 1, one would expect the wake to transition similar to the wake

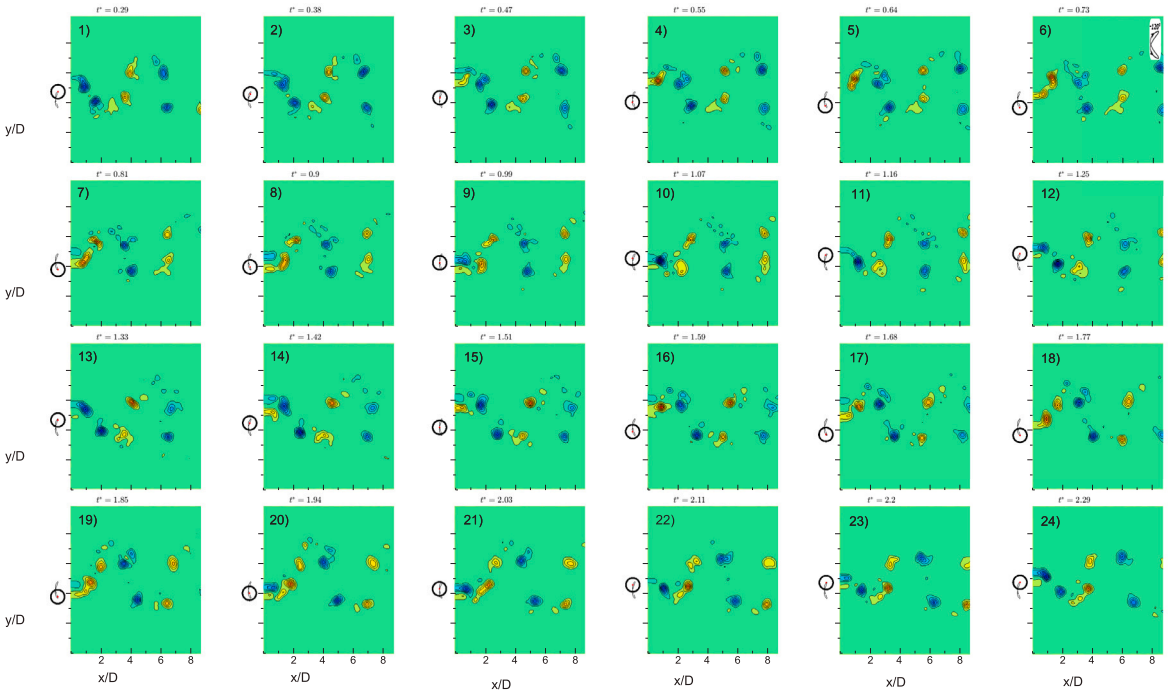

Fig. 14. Time history of wake vorticity for $A_y/D = 0.6$, $A_x/D = 0.1$, $V_r = 6$, $\theta = -120°$ corresponding to Branch 2 (upper surface of Fig. 12). Wake shows four vortices shed per cycle, similar to a '2*P*' shedding pattern, where vortices are paired with a counter-rotating partner. Vorticity contours show non-dimensional vorticity, $\frac{\omega D}{U}$. Supplemental video of this wake is provided online.

observed on Branch 1. In this case, a '2*S*' shedding pattern is a natural transitional state away from the previously observed '2*C*' pattern since if the co-rotating vortices merge into a single vortex, they would appear as a '2*S*' wake pattern.

To further demonstrate the presence of multi-branch regions, we highlight a second example. Fig. 17 shows C_{lv}, C_{la}, and C_{my} for $A_y/D = 1.1$, $A_x/D = 0.2$ and $\theta = -180$ °. In this case, the CF amplitude is significantly larger than the previous example. A branch occurs near $\theta = -180°$, but since we have repeated experiments for both $\theta = 180°$ and $\theta = -180°$, these are redundant motions and we can directly compare the repeated sets of experiments. As seen in the figure, experiments are again divided into a Branch 1 and Branch 2 set of experiments, however one interesting observation is that for the repeated experiments, the resulting force coefficient sometimes falls on the Branch 1 line and sometimes falls on the Branch 2 line, indicating that with repeated experiments in the branch region, we may randomly observe either branch. The measured force coefficients along each identified branch are also largely repeatable, showing smooth variation over V_r. The observability of both conditions in towing tank experiments is a testament to the quality of the experimental setup, where both conditions can be observed. Again, the presence of these distinct branch regions in the parameter space indicates a difference in the phasing between forces and motion of the body, which will occur for different wake organizations. For branch 1, we do observe a slight fluctuation in the measured force coefficients near $V_r = 7.8$, where the $-180°$ curve has a single data point that does not smoothly connect with the others. While we attribute this data point to branch 1, it is possible that additional branches exist, but were not observed in the present experiments, hence this point could belong to a different branch or could be a result of desynchronization at the higher V_r values.

To further illustrate the multiple branches over the entire range of θ, Fig. 18 shows a surface rendering of C_{la} for $A_y/D = 1.1$, $A_x/D = 0.2$. In this case, the separate branches are distinct at higher reduced velocities, rather than intersecting as with the previous case. It should be noted that since we separate the branch regions based purely on our observations, we are limited to identifying branches to where they were measured. It is certainly possible that the branch regions may exist over a larger range of reduced velocities, but if the experiments did not trigger a certain response to be observed, we have no way of knowing whether the region should be extended. Therefore, these plots should be carefully considered as only being based on the observed conditions from the experiments and not necessarily completely expansive in describing the observed phenomenon. We can again select particular wake visualizations to illustrate the wake differences between each of the separate branches.

For the wake with this set of motion parameters, there is significant variability to the measured vorticity in the wake, likely due to higher three-dimensionality of the wake for this specific combination of motion parameters. For this reason, instead of showing the raw time evolution of the wake, we show the phase-averaged wake, computed by phase averaging all measured cycles in bins of 10°, which helps identify distinguishing and dominant features of the wake. Fig. 19 shows a comparison of the phase averaged wake for the Branch 1 and Branch 2 wakes for $A_y/D = 1.1$, $A_x/D = 0.2$ and $\theta = -180$ °. The comparison is made for cases with $V_r = 5$ on Branch 2 and $V_r = 6$ on Branch 1. The left set of images correspond to the Branch 2 wake (upper surface from Fig. 18),

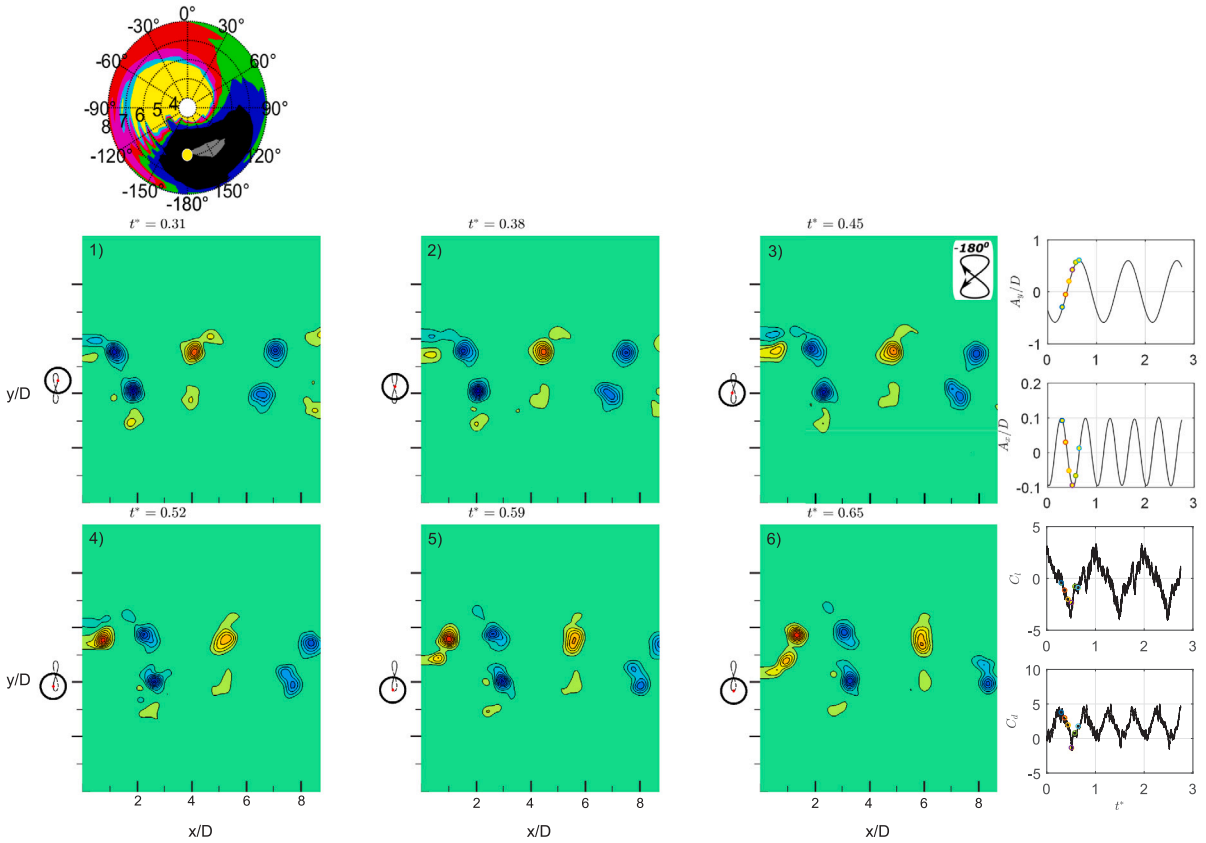

Fig. 15. Abbreviated time history of wake vorticity for $A_y/D = 0.6$ and $A_x/D = 0.1$, $V_r = 6$ and $\theta = -180°$. Vorticity contours show non-dimensional vorticity, $\frac{\omega D}{U}$. The yellow dot on the polar plot shows the location where the wake visualization is taken relative to the multi-branch region on Branch 2. The wake sheds four vortices per cycle with three strong vortices and one weak vortex. The resulting wake looks like an intermediate state between a symmetric '$2P$' type wake and an asymmetric '$P + S$' wake. Supplemental Video of this wake is provided online.

Table 4
Ranges of observed multi-branch regions in the database. It is expected that multiple wakes can form for these motion parameter conditions.

A_y/D	A_x/D	θ	V_r range
0.35	0.1	−120°	4.2–6.4
0.35	0.3	−120°	6.2–7.4
0.6	0.1	−120°	4.4–6.6
0.6	0.3	−120°	6.6–7.8
0.85	0.1	−150°	5.4–7.6
0.85	0.2	−120°	5.8–7.0
0.85	0.3	−120°	6.0–7.6
0.85	0.4	−120°	5.2–6.8
1.1	0.2	−180°	5.6–7.8
1.1	0.3	−150°	5.6–7.6
1.1	0.4	−150°	6.4–7.2
1.1	0.4	180°	7.4–7.8
1.1	0.5	−150°	6.8–7.6
1.35	0.2	−180°	4.2–7.8
1.35	0.3	−180°	6.0–7.8
1.35	0.4	−180°	4.8–8.0
1.35	0.5	−180°	7.4–7.8
1.6	0.3	150°	7.0–7.8

while the right set of images correspond to the phase averaged wake for Branch 1 (lower surface from Fig. 18). In the Branch 2 wake, a messy grouping of vorticity sheds to the wake of the cylinder initially, as indicated by the boxed regions in frames 1–3. The grouped vorticity is messy since it consists of multiple vortex structures that shed at the same time in the wake of the cylinder. As the grouping of vorticity propagates downstream, the vortex structures start to break apart, separating into distinct separate vortex structures further away from cylinder. This separation is illustrated by additional boxes shown in frames 4–6. In contrast, on Branch 1, distinct and separate like-signed vortices form in the near wake of the cylinder, as seen in frames 1–3 in the right set of images. As the vortices propagate downstream, the vortices coalesce into a single vortex structure. In both wakes, a similar set of vortices exist in the wake, however the phasing of vortex shedding results in two separate and distinct formations, where along Branch 2, there is a divergence or spreading of the vorticity in the wake, and along Branch 1, there is a coalescing of vorticity over time.

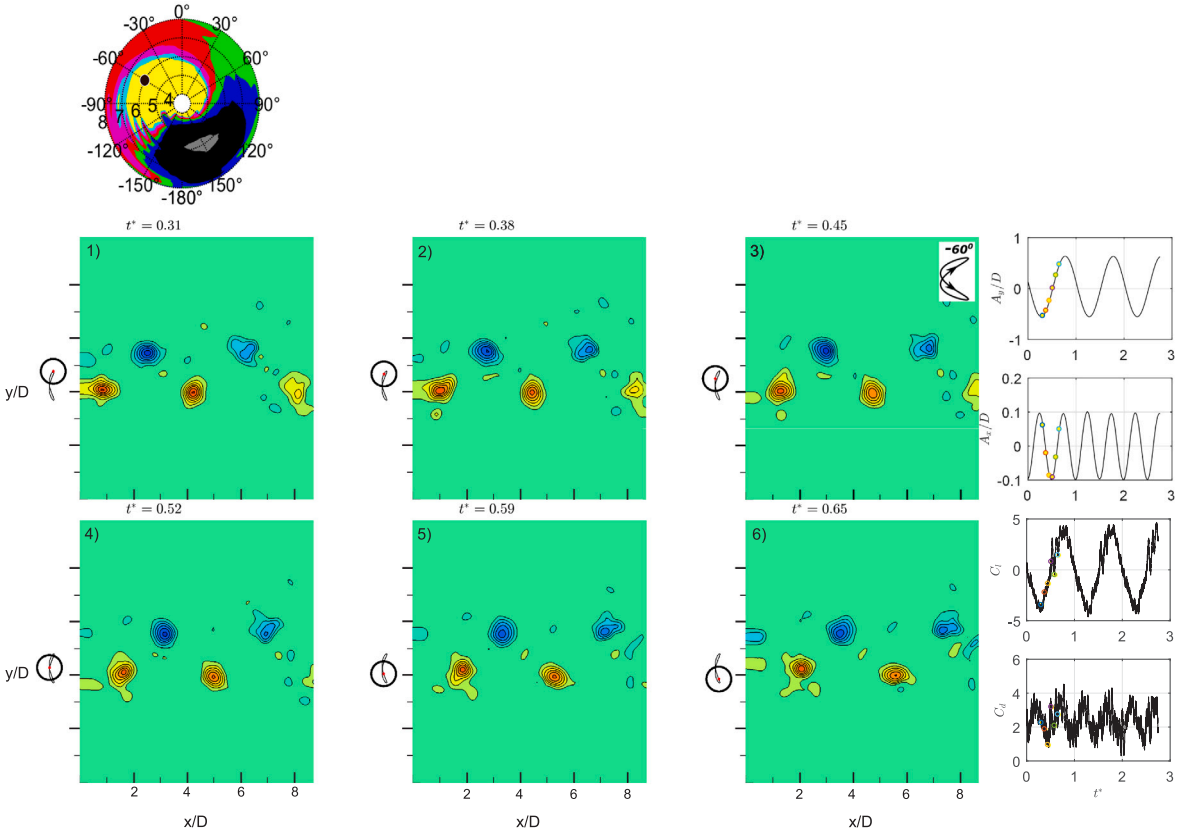

Fig. 16. Abbreviated time history of wake vorticity for $A_y/D = 0.6$ and $A_x/D = 0.1$, $V_r = 6$ and $\theta = -60°$. Vorticity contours show non-dimensional vorticity, $\frac{\omega D}{U}$. The black dot on the polar plot shows the location where the wake visualization is taken relative to the multi-branch region on Branch 1. The wake sheds two vortices per cycle typical of a '2*S*' type wake. The resulting wake looks like a transitional state from the observed Branch 1 '2*C*' wake. Supplemental Video of this wake is provided online.

Based on similar observable variability of force coefficients throughout the database, we identify all regions where multi-branch wakes potentially exist. Table 4 shows all observed multi-branch regions. It is significant that multi branch regions exist throughout the database, for a variety of amplitudes. One distinct observation is that all of these regions tend to exist in the lower left quadrant of the polar plots, with phases mostly between $\theta = -120°$ and $\theta = -180°$. Again, since these observations are largely made based on forced motion experiments conducted for a specific set of motion parameters, it is possible that some of the reported V_r ranges may not encompass the entire range where a multi-branch wake may exist. Additionally, increased resolution of all parameters, particularly θ and IL and CF amplitude, would help further resolve these regions.

4. Discussion

Overlapping multiple wake regions have been previously observed for forced CF motions in Morse and Williamson (2009b), where the small observed region corresponded to a transitional wake state between '2*S*' and '2*P*', called '$2P_O$'. This region exhibited a slightly different wake, with different phasing of vortex shedding and phase between the lift force and motion, such that two separate and distinct sets of force contours could be defined for a given combination of sinusoidal motion amplitude and frequency. In the present study, when considering combined IL and CF motion, the observation of these multiple possible wake regions is significantly enhanced due to the addition of the IL motion of the body. In addition, when considering the IL motion, the phase between IL and CF motion, θ, plays a significant role in the formation of the wake and phasing between forces and motion, such that we observe multiple branch regions of the wake throughout the tested dataspace.

The physical instability that is responsible for the observation of two different force branches and the corresponding different wakes is the same type of non-linear dynamic phenomenon observed in the free vibration of a 1-DOF system, as in Morse and Williamson (2009b). Although, in a forced motion experiment, the amplitude of motion or frequency of motion cannot change, the wake can, and multiple formations of the wake can still exist.

To observe a non-linear dynamic phenomenon with multiple solutions, we often rely on observing a hysteresis phenomenon in experiments, where the particular observed response of the system depends on the previous experimental conditions or direction at

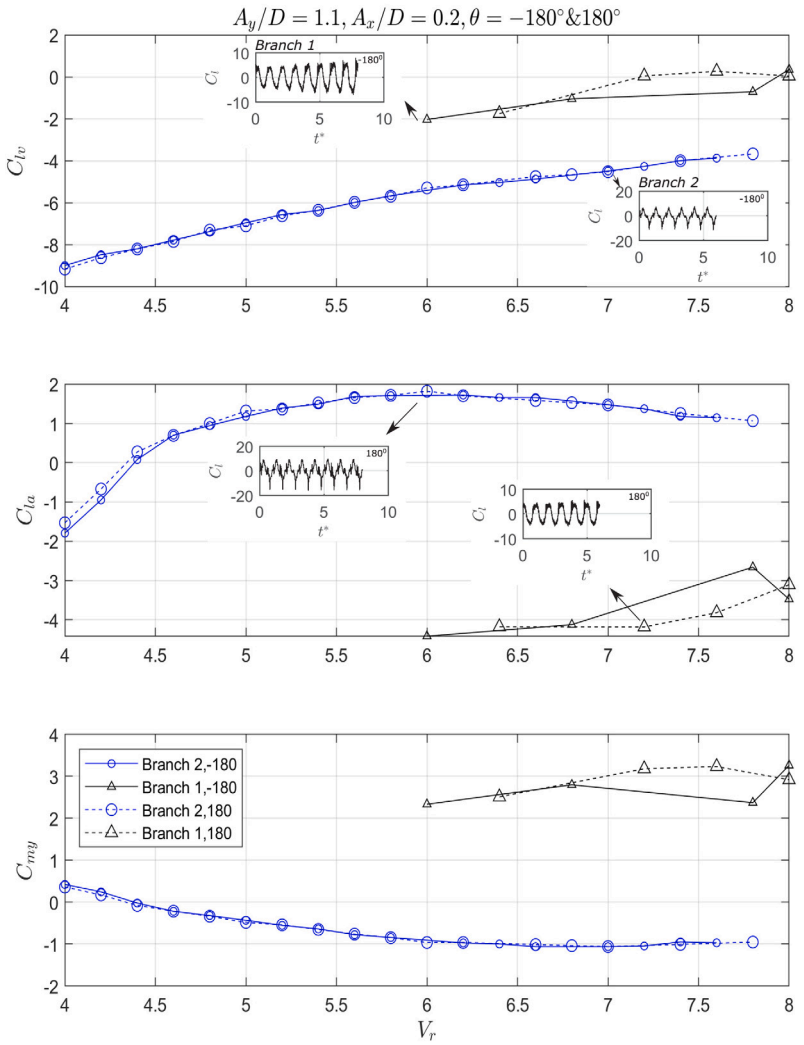

Fig. 17. Force coefficient branches observed for three hydrodynamic coefficients (C_{lv}, C_{la}, C_{my}) at $\theta = -180°$ and $\theta = 180$, $A_x/D = 0.2\&A_y/D = 1.1$. Branch 1 and branch 2 correspond to different wake conditions which result in variation of the phasing between motion and forcing, force amplitude, and variation in force coefficients. Repeated experiments demonstrate a consistent multi-branch response while some repeated experiments switched between the separate branches.

which an experimental parameter is varied (such as flow speed). However, it is not a necessity to observe hysteresis by approaching from a particular direction, hysteresis is simply a result of the way a phenomenon with multiple solutions is observed. In free vibration, 1-DOF experiments, if one conducts the experiment in a recirculating flow channel, then the direction at which one increases or decreases V_r does matter, since V_r is typically controlled by the flow speed in those experiments, and the cylinder would already be vibrating with an established wake, hence it's initial conditions bias the system to remain on the particular branch that it is already on. In contrast, if one conducted a towed experiment of the same free vibration system, the concept of approaching from a particular V_r does not matter, since if sufficient time has passed between experiments, the water is still and the cylinder is starting from rest. In this case, the system may always settle on the same particular branch if accelerated slowly or it might switch to a different branch dependent on the acceleration of the cylinder from rest or steadiness of the tow speed, hence it depends on the initial conditions for what one observes. If one randomly assumes an initial condition, the system will approach the nearest limit cycle and may switch between limit cycles if sufficient perturbations exist.

The fact that we observe different wakes for a given motion in the present experimental study would indicate that the wake may be sensitive to the initial conditions in the tank. This observation is no different than what is observed in Morse and Williamson (2009a), where forced motions are performed for a 1-DOF system and multiple possible wakes and forces exist ('$2P_O$' or '$2S$', or '$2P_O$' or '$2P$') in a overlapping region of the amplitude-V_r map. In Morse and Williamson (2009a), these multiple branches were observed by conducting experiments in a recirculating flow channel over a large number of cycles, where switching of the wake mode would intermittently occur for a given forced motion. It is worth noting that observing mode switching may necessitate a

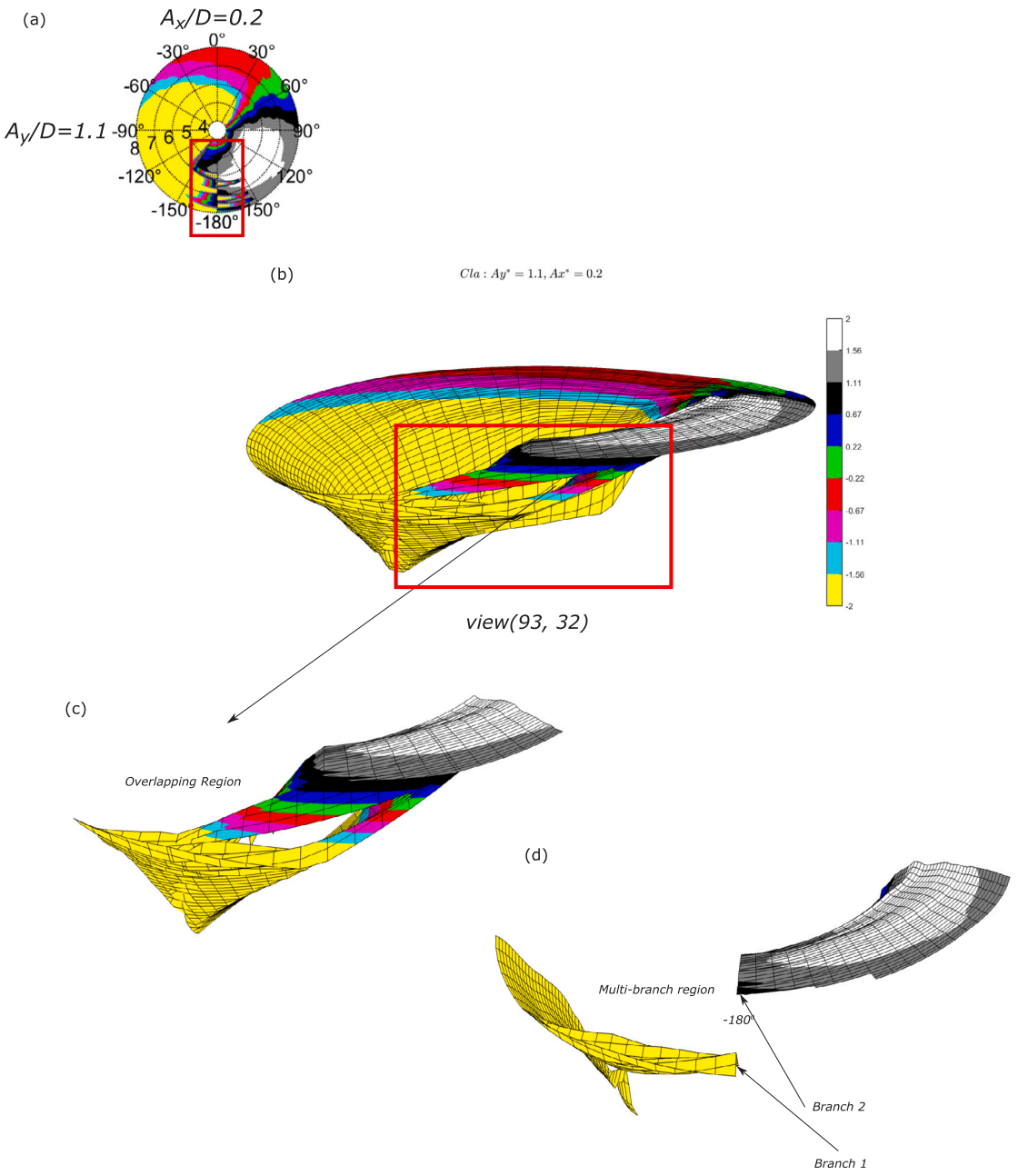

Fig. 18. Illustration of multiple branches in the polar contour plot of the lift force coefficient in phase with acceleration, C_{la}, for fixed $A_y/D = 1.1$, $A_x/D = 0.2$, and over the entire tested range of θ and V_r. Branches 1 and 2 are identified according to the same branches labeled in Fig. 17. (a) Polar plot of C_{la} for the given motion conditions, red box indicates the region where multiple branches are observed. (b) 3-D surface plot view of the same polar plot in (a) to illustrate the region where multiple branches overlap one another, the red box shows the same multiple branch region as in (a). (c) Cutaway view of only the overlapping multi-branch region to help illustrate the multi-branch region.(d) Cutaway of the multi-branch region at $\theta = -180°$, edge surfaces correspond to the lines shown in Fig. 17.

longer time history of oscillations and we do not observe it in this work. One may also argue that with a limited number of forced motion cycles in the present experiments, the wake may not have achieved dynamic equilibrium yet; however, the following three reasons suggest that the wake has reached dynamic equilibrium in these experiments:

1. If we compute hydrodynamic coefficients on a cycle by cycle basis, we observe very steady values that do not significantly change over the length of the experiment. This is observed in both cases with and without branches, indicating that in the present experiments, when a wake is developed on a particular branch, it remains on that branch.

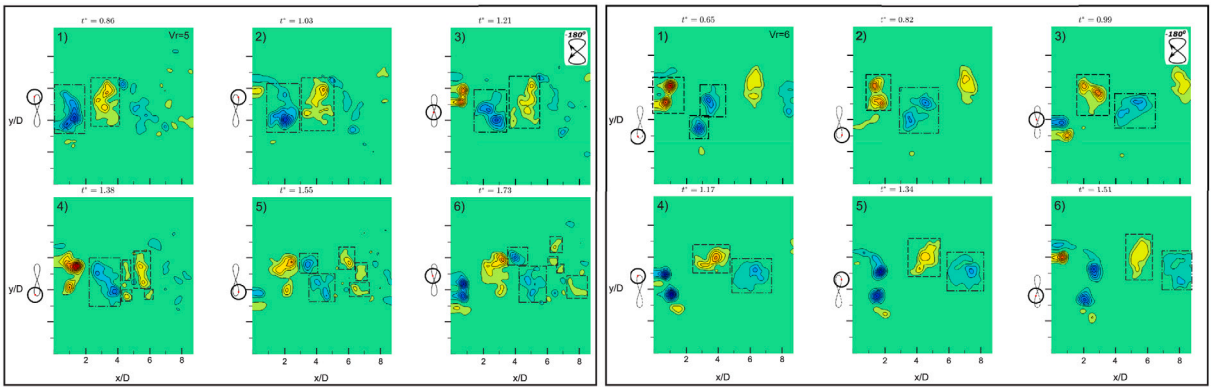

Fig. 19. Phase averaged wake vorticity for $A_y/D = 1.1$, $A_x/D = 0.2$, $V_r = 5$, $\theta = -180°$ (left) corresponding to Branch 2 and $A_y/D = 1.1$, $A_x/D = 0.2$, $V_r = 6$, $\theta = -180°$ (right) corresponding to Branch 1. Vorticity contours show non-dimensional vorticity, $\frac{\omega D}{U}$. Branch 2 demonstrates a diverging set of vortices that spread apart into distinct, smaller vortex structures as the wake propagates in space and time. Branch 1 demonstrates a coalescing set of vortices that combine as the wake propagates in time and space. Supplemental Video of these wakes are provided online.

2. Each data point shown in the present experiments is for a completely separate experiment, where we wait for the tank to settle for about 8.5 min, then conduct a new experiment. Due to wait times in the automated experiments, the actual time the water is allowed to settle is about 10 min. If we consider what is happening to force coefficients, such as C_{lv}, from experiment to experiment, we can see that the transition of this value is smooth between experiments when there is not a branch. For example, the top image in Fig. 17 shows C_{lv} as a function of reduced velocity for a particular fixed IL amplitude, CF amplitude, and phase difference between IL and CF motions. The solid blue line shows a series of experiments with a very smooth transition in C_{lv} between experiments at low reduced velocity. Consequently, the dashed blue line shows the same experiments repeated, demonstrating there is little to no variation in the observed C_{lv} when there are not multiple branches, as occurs here at low reduced velocity. At higher reduced velocity, a branch occurs. Splitting the data into the different branches shows that the variation in C_{lv} along the branch is still smooth, indicating that the mean values that are calculated from the cycle by cycle value of C_{lv} are still smooth across experiments, even when some of the experiments show a slight variation in the value of C_{lv} over time. Additionally, by repeating the experiments, there are cases, for the exact same motion parameters and reduced velocity, where either one branch or the other is observed, not intermediate values.
3. In many of the observed experiment cases, there is a clear, large difference in the values of the force coefficients on the branch. Taking Fig. 17 as an example again, the difference between C_{la} on each branch is very large: 1 on the upper branch and −4 on the lower branch. Again, we do not observe intermediate values of the coefficient for different experiments, as one might expect if the wake was still in a transient state, so we believe that one can conclude these branches do exist. Certainly there may be some uncertainty in whether the exact reported values of C_{lv} and C_{la} are correct if some evolution of the wake is still occurring, but the presence of the branches is a real phenomenon.

While Figs. 7, 8, and 9 show examples of force coefficient contours observed in the present experimental study and can give an idea of regions where energy transfer occurs between the fluid and structure and vice versa, this is not the conventional way of showing this type of information, as in Morse and Williamson (2009b) or Gopalkrishnan (1993), where force contours may be shown as a function of A_y/D versus V_r. We illustrate the data this way due to the discretization of the experiments, where there is more resolution in θ and V_r than in the amplitude parameters, hence these figures show the most compact way to illustrate force coefficients for the entire database. However, if we want to make comparisons with 1-DOF motion studies, it is necessary to view the dataspace in a more conventional form. Fig. 20 shows contours of C_{lv} plotted as a function of A_y/D on the vertical axis and V_r on the horizontal axis for a select number of motion parameters.

In Fig. 20, we only show a small subspace of the database in this way for comparison purposes, where the specific fixed parameters of $\theta = [-30°, 0°]$ and $A_x/D = [0.1, 0.2, 0.3]$ are chosen since these values correspond to similar amplitudes and phases that might be observed in the free vibration of a 2-DOF elastically mounted cylinder system (Jauvtis and Williamson, 2004; Dahl et al., 2006, 2010). When shown this way, we can immediately see the separate bounded white region, where C_{lv} takes positive values. This bounded region shows the space where the wake exerts an excitation force on the body, depending on the mechanical damping of the system. A theoretical system with zero mechanical damping would oscillate with amplitude and reduced velocity along the curve of $C_{lv} = 0$. The gray region shows areas where C_{lv} is negative, where the fluid provides a damping force that will reduce the amplitude of motion. A freely vibrating cylinder by itself would not oscillate with amplitude and frequency combinations in this region as the fluid forcing would drive the system towards the white regions. It should be noted that each subfigure is shown for a fixed combination of phase lag between IL and CF motion, θ, and IL amplitude A_x/D, hence a freely vibrating system would be capable of exhibiting responses in any of the white regions, including regions in between these curves that cannot be shown without interpolation across θ or A_x/D. Additionally, the specific amplitude and frequency at which a freely vibrating system oscillates would depend on the specific mass of the system in the x and y directions along with the specific damping of the system in the x and y

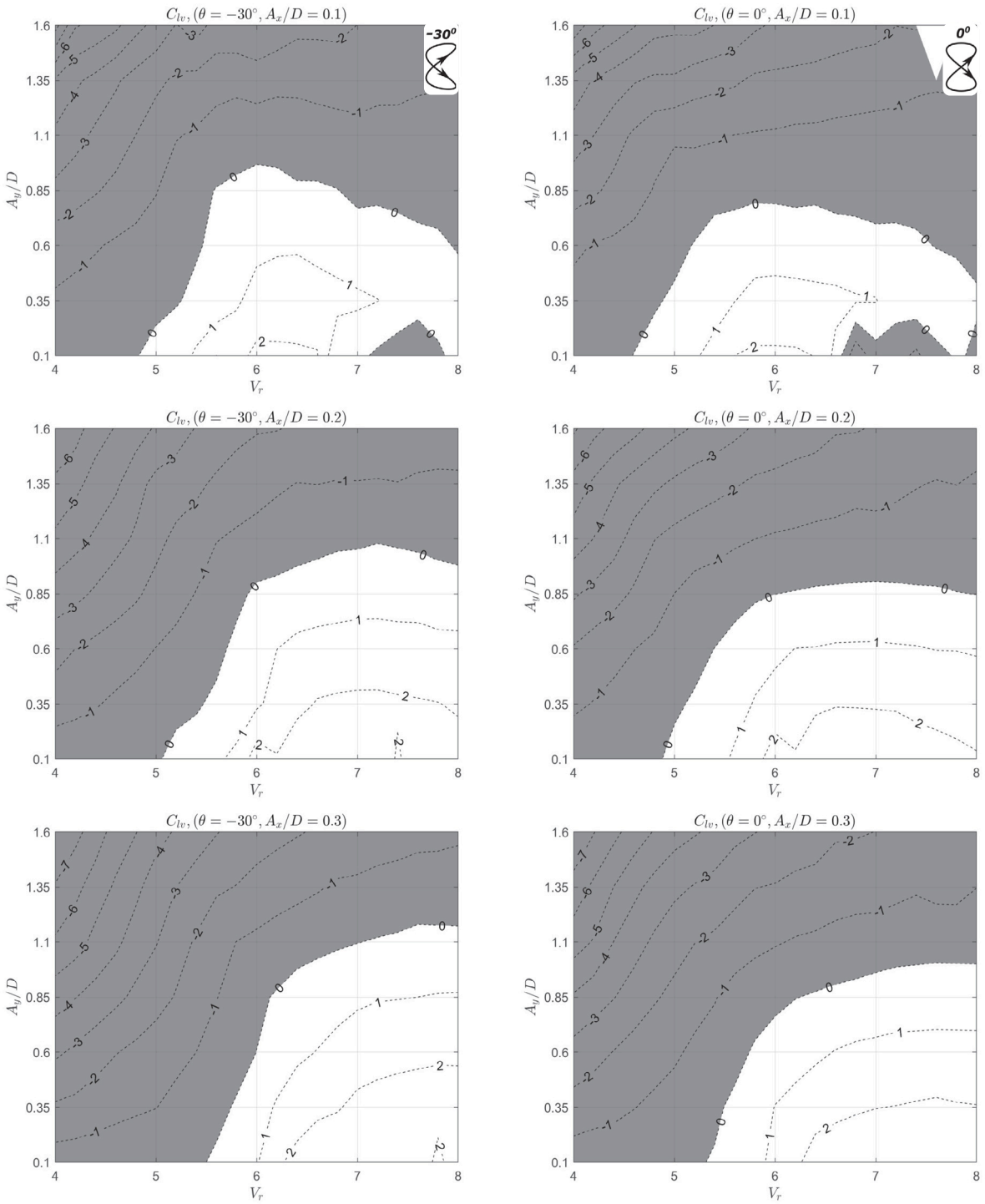

Fig. 20. Contours of lift coefficient in phase with velocity, C_{lv} as a function of CF amplitude, A_y/D and reduced velocity, V_r. Left figures show contours for fixed phase, $\theta = -30°$ and right figures show contours for fixed phase, $\theta = 0°$. From top to bottom, figures show fixed values of IL amplitude with $A_x/D = 0.1$, 0.2, 0.3. White regions indicate areas where C_{lv} is positive, indicating an excitation region where there is net energy transfer from the fluid to the body. Gray regions show where C_{lv} is negative, indicating a damping region where there is net energy transfer from the body to the fluid.

directions. For example, freely vibrating systems with the same mass damping characteristics in x and y (Jauvtis and Williamson, 2004) will exhibit a different response than a freely vibrating system with different mass and damping characteristics in x and y (Dahl et al., 2006). We can see from comparison of these subfigures that the white excitation region shifts to higher reduced velocities as the IL amplitude becomes larger and the slight change in phase has a small effect on the extents of the excitation region in CF motion.

From Fig. 20 we can make some observations in comparison with freely vibrating systems. In Jauvtis and Williamson (2004) and Dahl et al. (2006), both studies observed very large amplitude responses, greater than $A_y/D = 1.3$ for θ around a value of $-90°$ (the specific value of θ does vary depending on the reduced velocity), but for motions with $\theta = 0°$, the response was smaller, closer to $A_y/D = 0.8$, which is consistent with the observed white regions in Fig. 20. While the particular combination of motion parameters in Fig. 20 do not show a multi-branch wake region, Jauvtis and Williamson (2004) did observe a hysteretic response for V_r between 6.5 and 7.5, characterized by an upper branch and lower branch, where the upper branch exhibited phases around $\theta = -90°$ and $A_x/D \approx 0.1$, with the lower branch exhibiting nearly no IL motion. This region does not quite exist in the current database since the smallest IL motions conducted in the current study were for $A_x/D = 0.1$, however as seen in Table 4, we do observe multi-branch regions with large CF amplitude, small IL amplitude and similar θ, however it is likely that even with the present resolution, the database is still not sufficiently resolved to illustrate all possible multiple branch regions. In addition to resolution, by conducting a towed experiment, we are limited by the length of the tank and the initial conditions of the experiment, hence we are not guaranteed to observe all multiple branch regions as might be possible with longer experiments conducted in a longer tank or recirculating flow channel.

In regards to the observation of multiple branch regions, Cagney and Balabani (2014) found that for a freely oscillating cylinder in purely IL motion, multiple response branches exist for different ranges of reduced velocities, and multiple modes are possible within specific response branches, however, when CF motion was allowed, the addition of CF motion resulted in only a single wake mode being observed, with no hysteresis. This observation is not inconsistent with the observations of the present study, as we note that hysteresis may only possibly occur in cases where multiple force branches exist and as seen in the present study, these branch regions primarily exist for cylinder phases that are not typically observed for a rigid cylinder elastically mounted to springs. However, for continuously flexible cylinders, such as a drilling riser, pipeline, or towed cable for example, where the response of the cylinder can vary along its span, it is possible to have power in and power out regions along the span of the body (Swithenbank and Vandiver, 2007), in which case, phases with multiple branches may be excited in the resulting response of the structure. In a case like this, an accurate prediction of the structure's response may be difficult as one would not know which branch may be excited a priori. It is likely that the wake would be highly dependent on the three-dimensionality of the system, hence the specific branch that is excited on the flexible structure may be dependent on how the near neighboring wake has formed.

This is not a trivial observation, since it indicates that prediction of the response of a vibrating system undergoing combined IL and CF motion is complicated by a non-unique wake condition for a given response. It must be noted as well that the present study considers the measured forces over a fixed Reynolds number of 7620. Reynolds number is known to alter the separation condition on shedding vortices and the force magnitude, where variation of multiple branch regions as a function of Reynolds number is not known. While conducting massively large sets of experiments to investigate such phenomena can be informative, it is likely unfeasible to extend such experimental databases over a significant range of Reynolds numbers and more sophisticated methods for exploring the data space may be necessary, such as those proposed in Fan et al. (2019b). Even then, careful evaluation of massive sets of data to observe phenomena such as multiple branch regions can be elusive, even for sophisticated machine learning techniques.

In addition to the presence of multiple branch regions in the present study, the observed variation of the wake in these regions demonstrates a complicated nature to wake formation when IL and CF motion is combined. The observed wake conditions appear to be closely related to the well characterized CF wake modes, although variations and transitions away from these standard wake modes appear to be ubiquitously present in the current database. A more detailed evaluation of how IL wake modes, such as those characterized in Cagney and Balabani (2013a), and CF wake modes as in Williamson and Roshko (1988) may interact for different phasing of IL and CF motion is necessary and beyond the scope of the present paper. A separate paper related to wake visualization in the present study is necessary.

The observation of multiple branch regions in the present study is interesting by the fact that it is observed while conducting a series of towing tank experiments, where the experiment starts from a still tank condition. While hysteresis and multiple wake responses have been observed in forced motion in Morse and Williamson (2009b), free vibration studies in Govardhan and Williamson (2000), and flexible cylinder studies (Gedikli and Dahl, 2017; Gedikli et al., 2018), these observations are typically made in recirculating flow channels, where the experiments can be conducted over much longer periods of time and a particular branch is approached by increasing or decreasing the flow speed within the flow channel, or mode switching may be observed in the case of freely vibrating systems. It is interesting to note in the present experiments, that when experiments are repeated (as in cases with $\theta = 180°$), we sometimes observe the same response and we sometimes observe the alternate branch response. This indicates that the experiments either have no bias that would tend towards a particular branch, or that there is still some low level disturbance present in the tank that could trigger the system to switch between branch conditions, since our experiments are always performed in exactly the same way (i.e. motion always begins by moving in the same y-direction although the x-direction will depend on phase). Since the experiments are automated, such that they are repeated in exactly the same way with the same waiting time of 8.5 min between experiments, it seems unlikely that disturbances are present in the tank that could cause a switch between observed branches, although it is possible. Additionally, since the response branches are observed as a function of the phase, θ, we are limited to observing these branches based on the resolution of θ along with what is observed in the experiment itself. As noted earlier, it is possible that additional branches exist, but were not observed in the present study, or were not observed to the extent

to be identified as an additional branch. Due to the already large set of data encompassing this current set of experiments, tripping of specific response branches and higher resolution of these response branches were not investigated, but could be investigated in future studies, possibly through more sophisticated experiment selection or through numerical experiments.

5. Conclusion

To summarize the present study, we present observations of the measured forces and wakes for a cylinder that is towed at forward speed and forced to undergo sinusoidal motions in the CF and IL directions. We provide a mapping of the decomposed fluid hydrodynamic force coefficients over the entire range of the tested parameter space, which consists of variation of the IL amplitude, CF amplitude, reduced velocity, and the phase between IL and CF motions. From force measurements, we conclude that IL motion has the effect of enhancing the CF response of a system that undergoes this type of combined motion. For specific combinations of motion parameters, multiple branch regions were observed where the wake and resulting forces can demonstrate two distinct values for a given set of motion conditions. These multiple branch regions exhibit distinct wake characteristics that correspond to changes in the phasing between forces acting on the cylinder and motions of the cylinder. In contrast to systems restricted to only CF motions, these multiple branch regions are observed throughout a large space of motions within the database, indicating a wide region where multiple stable wakes may exist for a given set of cylinder motions.

Declaration of competing interest

The authors declare that they have no known competing financial interests or personal relationships that could have appeared to influence the work reported in this paper.

Data availability

Data will be made available on request.

Appendix A. Supplementary data

Supplementary material related to this article can be found online at https://doi.org/10.1016/j.jfluidstructs.2023.104035.

References

Aktosun, E., Dahl, J., 2018. Experimental force database from controlled in-line and cross flow cylinder motion. In: The 28th International Ocean and Polar Engineering Conference. International Society of Offshore and Polar Engineers, pp. 1019–2026.

Aronsen, K., 2007. An Experimental Investigation of In-Line and Combined In-Line and Cross-Flow Vortex Induced Vibrations (Ph.D. thesis). Norwegian University of Science and Technologhy.

Bearman, P., 1984. Vortex shedding from oscillating bluff bodies. Annu. Rev. Fluid Mech. 16 (1), 195–222.

Bearman, P., 2009. Understanding and predicting vortex-induced vibrations. J. Fluid Mech. 634, 1–4.

Bearman, P., 2011. Circular cylinder wakes and vortex-induced vibrations. J. Fluids Struct. 27 (5–6), 648–658.

Bishop, R., Hassan, A., 1964a. The lift and drag forces on a circular cylinder in a flowing fluid. Proc. R. Soc. Lond. Ser. A. Math. Phys. Sci. 277 (1368), 32–50.

Bishop, R., Hassan, A., 1964b. The lift and drag forces on a circular cylinder oscillating in a flowing fluid. Proc. R. Soc. Lond. Ser. A. Math. Phys. Sci. 277 (1368), 51–75.

Bourguet, R., Karniadakis, G.E., Triantafyllou, M.S., 2011. Vortex-induced vibrations of a long flexible cylinder in shear flow. J. Fluid Mech. 677, 342?382. http://dx.doi.org/10.1017/jfm.2011.90.

Cagney, N., Balabani, S., 2013a. On multiple manifestations of the second response branch in streamwise vortex-induced vibrations. Phys. Fluids 25 (7), 075110. http://dx.doi.org/10.1063/1.4816293.

Cagney, N., Balabani, S., 2013b. Wake modes of a cylinder undergoing free streamwise vortex-induced vibrations. J. Fluids Struct. 38, 127–145. http://dx.doi.org/10.1016/j.jfluidstructs.2012.12.004.

Cagney, N., Balabani, S., 2014. Streamwise vortex-induced vibrations of cylinders with one and two degrees of freedom. J. Fluid Mech. 758, 702–727. http://dx.doi.org/10.1017/jfm.2014.521.

Cagney, N., Balabani, S., 2016. Fluid forces acting on a cylinder undergoing streamwise vortex-induced vibrations. J. Fluids Struct. 62, 147–155. http://dx.doi.org/10.1016/j.jfluidstructs.2016.01.007.

Chaplin, J., Bearman, P., Cheng, Y., Fontaine, E., Graham, J., Herfjord, K., F.J., H.-H., Isherwood, M., Lambrakos, K., Larsen, C., 2005. Blind predictions of laboratory measurements of vortex-induced vibrations of a tension riser. J. Fluids Struct. 21 (1), 25–40.

Dahl, J., 2008. Vortex-Induced Vibration of a Circular Cylinder with Combined In-Line and Cross-Flow Motion (Ph.D. thesis). Massachusetts Institute of Technology, Cambridge, MA.

Dahl, J., Hover, F., Triantafyllou, M., 2006. Two-degree-of-freedom vortex-induced vibrations using a force assisted apparatus. J. Fluids Struct. 22 (6–7), 807–818.

Dahl, J., Hover, F., Triantafyllou, M., Dong, S., Karniadakis, G., 2007. Resonant vibrations of bluff bodies cause multivortex shedding and high frequency forces. Phys. Rev. Lett. 99 (14), 144–503.

Dahl, J., Hover, F., Triantafyllou, M., Oakley, O., 2010. Dual resonance in vortex-induced vibrations at subcritical and supercritical Reynolds numbers. J. Fluid Mech. 643, 395–424.

Fan, D., Jodin, G., Consi, T.R., Bonfiglio, L., Ma, Y., Keyes, L.R., Karniadakis, G.E., Triantafyllou, M.S., 2019a. A robotic Intelligent Towing Tank for learning complex fluid-structure dynamics. Science Robotics 4 (36), eaay5063. http://dx.doi.org/10.1126/scirobotics.aay5063.

Fan, D., Jodin, G., Consi, T.R., Bonfiglio, L., Ma, Y., Keyes, L.R., Karniadakis, G.E., Triantafyllou, M.S., 2019b. A robotic Intelligent Towing Tank for learning complex fluid-structure dynamics. Science Robotics 4 (36), http://dx.doi.org/10.1126/scirobotics.aay5063.

Fan, D., Triantafyllou, M.S., 2022. Vortex-induced forces of crossflow and inline oscillating bluff bodies at moderate Reynolds numbers. Mar. Struct. 86, 103305. http://dx.doi.org/10.1016/j.marstruc.2022.103305.

Fan, D., Wang, Z., Triantafyllou, M.S., Karniadakis, G., 2019c. Mapping the properties of the vortex-induced vibrations of flexible cylinders in uniform oncoming flow. J. Fluid Mech. 881, 815–858.
Flemming, F., Williamson, C., 2005. Vortex-induced vibrations of a pivoted cylinder. J. Fluid Mech. 522, 215–252.
Gabbai, R., Benaroya, H., 2005. An overview of modeling and experiments of vortex-induced vibration of circular cylinders. J. Sound Vib. 282 (3–5), 575–616.
Gedikli, E.D., Chelidze, D., Dahl, J.M., 2018. Observed mode shape effects on the vortex-induced vibration of bending dominated flexible cylinders simply supported at both ends. J. Fluids Struct. 81, 399–417. http://dx.doi.org/10.1016/j.jfluidstructs.2018.05.010.
Gedikli, E.D., Dahl, J.M., 2017. Mode excitation hysteresis of a flexible cylinder undergoing vortex-induced vibrations. J. Fluids Struct. 69, 308–322.
Gopalkrishnan, R., 1993. Vortex-Induced Forces on Oscillating Bluff Cylinders. Technical Report, Woods Hole Oceanographic Institution, MA.
Govardhan, R., Williamson, C., 2000. Modes of vortex formation and frequency response of a freely vibrating cylinder. J. Fluid Mech. 420, 85–130.
Gurian, T.D., Currier, T., Modarres-Sadeghi, Y., 2019. Flow force measurements and the wake transition in purely inline vortex-induced vibration of a circular cylinder. Phys. Rev. Fluids 4, 034701. http://dx.doi.org/10.1103/PhysRevFluids.4.034701.
Jauvtis, N., Williamson, C., 2004. The effect of two degrees of freedom on vortex-induced vibration at low mass and damping. J. Fluid Mech. 509, 23–62.
Jeon, D., Gharib, M., 2001. On circular cylinders undergoing two-degree-of-freedom forced motions. J. Fluids Struct. 15 (3–4), 533–541. http://dx.doi.org/10.1006/jfls.2000.0365.
Kang, Z., Jia, L., 2013. An experiment study of a cylinder's two degree of freedom VIV trajectories. Ocean Eng. 70, 129–140.
Konstantinidis, E., 2014. On the response and wake modes of a cylinder undergoing streamwise vortex-induced vibration. J. Fluids Struct. 45, 256–262. http://dx.doi.org/10.1016/j.jfluidstructs.2013.11.013.
Moe, G., Wu, Z.-J., 1990. The lift force on a cylinder vibrating in a current. J. Offshore Mech. Arct. Eng. 112 (4), 297–303. http://dx.doi.org/10.1115/1.2919870.
Morse, T., Williamson, C., 2009a. Fluid forcing, wake modes, and transitions for a cylinder undergoing controlled oscillations. J. Fluids Struct. 25 (4), 697–712.
Morse, T., Williamson, C., 2009b. Prediction of vortex-induced vibration response by employing controlled motion. J. Fluid Mech. 634, 5–39.
Mukundan, H., Modarres-Sadeghi, Y., Dahl, J., Hover, F.S., Triantafyllou, M., 2009. Monitoring VIV fatigue damage on marine risers. J. Fluids Struct. 25 (4), 617–628.
Peppa, S., Kaiktsis, L., Frouzakis, C.E., Triantafyllou, G.S., 2021. Computational study of three-dimensional flow past an oscillating cylinder following a figure eight trajectory. Fluids 6 (3), http://dx.doi.org/10.3390/fluids6030107.
Prasanth, T.K., Premchandran, V., Mittal, S., 2011. Hysteresis in vortex-induced vibrations: Critical blockage and effect of M. J. Fluid Mech. 671, 207–225, Cited By :31.
Sarpkaya, T., 1979. Vortex-induced oscillations: A selective review. J. Appl. Mech. 46 (2), 241–258. http://dx.doi.org/10.1115/1.3424537.
Sarpkaya, T., 1995. Hydrodynamic damping, flow-induced oscillations, and biharmonic response. J. Offshore Mech. Arct. Eng. 117 (4), 232–238.
Sarpkaya, T., 2004. A critical review of the intrinsic nature of vortex-induced vibrations. J. Fluids Struct. 19 (4), 389–447.
Sarpkaya, T.S., 2010. Wave Forces on Offshore Structures. Cambridge University Press, http://dx.doi.org/10.1017/CBO9781139195898.
Smogeli, O., 2002. Design and Evaluation of a Force-Feedback Control System for VIV Experiments. NTNU, MIT.
Srinil, N., Zanganeh, H., Day, A., 2013. Two-degree-of-freedom VIV of circular cylinder with variable natural frequency ratio: Experimental and numerical investigations. Ocean Eng. 73, 179–194. http://dx.doi.org/10.1016/j.oceaneng.2013.07.024.
Staubli, T., 1983. Calculation of the vibration of an elastically mounted cylinder using experimental data from forced oscillation. J. Fluids Eng.
Swithenbank, S.B., Vandiver, J.K., 2007. Identifying the power-in region for vortex-induced vibrations of long flexible cylinders. In: Proceedings of the ASME 2007 26th International Conference on Offshore Mechanics and Arctic Engineering. In: International Conference on Offshore Mechanics and Arctic Engineering, pp. 723–730. http://dx.doi.org/10.1115/OMAE2007-29156.
Triantafyllou, M., Bourguet, R., Dahl, J., Modarres-Sadeghi, Y., 2016. Vortex-induced vibrations. In: Dhanak, M., Xiros, N. (Eds.), Springer Handbook of Ocean Engineering. Springer Cham, Berlin, Germany, pp. 819–850.
Vikestad, K., Vandiver, J., Larsen, C., 2000. Added mass and oscillation frequency for a circular cylinder subjected to vortex-induced vibrations and external disturbance. J. Fluids Struct. 14 (7), 1071–1088.
Wang, J.-s., Fan, D., Lin, K., 2020. A review on flow-induced vibration of offshore circular cylinders. J. Hydrodyn. 32 (3), 415–440.
Williamson, C., Govardhan, R., 2004. Vortex-induced vibrations. Annu. Rev. Fluid Mech. 36, 413–455.
Williamson, C., Roshko, A., 1988. Vortex formation in the wake of an oscillating cylinder. J. Fluids Struct. 2 (4), 355–381.
Zheng, H., Dahl, J., Modarres-Sadeghi, Y., Triantafyllou, M., 2014a. Coupled inline-cross flow VIV hydrodynamic coefficients database. In: ASME 2014 33rd International Conference on Ocean, Offshore and Arctic Engineering. American Society of Mechanical Engineers, V002T08A087.
Zheng, H., Price, R., Modarres-Sadeghi, Y., Triantafyllou, M., 2014b. On fatigue damage of long flexible cylinders due to the higher harmonic force components and chaotic vortex-induced vibrations. Ocean Eng. 88, 318–329.